THERMALLY STIMULATED CURRENT STUDY OF TRAPS
DISTRIBUTION IN BETA-TlInS$_2$ LAYERED CRYSTALS

A THESIS SUBMITTED TO
THE GRADUATE SCHOOL OF NATURAL AND APPLIED SCIENCES
OF
MIDDLE EAST TECHNICAL UNIVERSITY

BY

MEHMET IŞIK

IN PARTIAL FULFILLMENT OF THE REQUIREMENTS
FOR
THE DEGREE OF MASTER OF SCIENCE
IN
PHYSICS

JUNE 2008

Approval of the thesis:

THERMALLY STIMULATED CURRENT STUDY OF TRAPS DISTRIBUTION IN BETA-TlInS$_2$ LAYERED CRYSTALS

submitted by **MEHMET IŞIK** in partial fulfillment of the requirements for the degree of **Master of Science in Physics Department**, **Middle East Technical University** by,

Prof. Dr. Canan Özgen
Dean, Graduate School of **Natural and Applied Sciences**　　　　———————

 Prof. Dr. Sinan Bilikmen
Head of Department, **Physics**　　　　———————

Assoc. Prof. Dr. Enver Bulur
Supervisor, **Physics Dept., METU**　　　　———————

Examining Committee Members

Prof. Dr. Bahtiyar Salamov
Physics Dept., Gazi University　　　　———————

Assoc. Prof. Dr. Enver Bulur
Physics Dept., METU　　　　———————

Prof. Dr. Nizami Hasanli
Physics Dept., METU　　　　———————

Prof. Dr. Gülay Öke
Physics Dept., METU　　　　———————

Assoc. Prof. Dr. Hatice Kökten
Physics Dept., METU　　　　———————

Date:　　<u>10　Haziran　2008</u>

ii

I hereby declare that all information in this document has been obtained and presented in accordance with academic rules and ethical conduct. I also declare that, as required by these rules and conduct, I have fully cited and referenced all materials and results that are not original to this work.

Name, Last Name : Mehmet Işık

Signature　　　　　:

ABSTRACT

THERMALLY STIMULATED CURRENT STUDY OF TRAPS DISTRIBUTION IN BETA-TlInS$_2$ LAYERED CRYSTALS

Işık, Mehmet

M. S., Department of Physics

Supervisor: Assoc. Prof. Dr. Enver Bulur

June 2008, 80 pages

Trapping centres in as-grown TlInS$_2$ layered single crystals have been studied by using a thermally stimulated current (TSC) technique. TSC measurements have been performed in the temperature range of 10-300 K with various heating rates. Experimental evidence has been found for the presence of five trapping centres with activation energies 12, 14, 400, 570 and 650 meV. Their capture cross-sections and concentrations were also determined. It is concluded that in these centres retrapping is negligible as confirmed by the good agreement between the experimental results and the theoretical predictions of the model that assumes slow retrapping. An exponential distribution of traps was revealed from the analysis of the TSC data obtained at different light excitation temperatures.

The transmission and reflection spectra of TlInS$_2$ crystals were measured over the spectral region of 400-1100 nm to determine the absorption coefficient

and refractive index. The analysis of the room temperature absorption data revealed the coexistence of the indirect and direct transitions. The absorption edge was observed to shift toward the lower energy values as temperature increases from 10 to 300 K. The oscillator and the dispersion energies, and the zero-frequency refractive index were also reported. Furthermore, the chemical composition of $TlInS_2$ crystals was determined from energy dispersive spectroscopic analysis. The parameters of monoclinic unit cell were found by studying the x-ray powder diffraction.

Keywords: Layered Semiconductors, Thermally Stimulated Currents, Electrical Properties, Defects, X-ray Diffraction, Energy Dispersive Spectral Analysis, Photoconductivity, Optical Constants.

ÖZ

BETA-TlInS$_2$ KATMANLI KRİSTALLERDE TUZAK DAĞILIMLARININ ISILUYARILMIŞ AKIM ÇALIŞMASI

Işık, Mehmet

Yüksek Lisans, Fizik Bölümü

Tez Yöneticisi: Doç. Dr. Enver Bulur

Katkılanmamış TlInS$_2$ katmanlı kristallerindeki tuzak seviyelerinin araştırılması ısıluyarılmış akım ölçümleri kullanılarak gerçekleştirildi. Isıluyarılmış akım ölçümleri 10-300 K sıcaklık aralığında, farklı ısıtma hızları ile yapıldı. Deneysel veriler aktivasyon enerjileri 12, 14, 400, 570 ve 650 meV olan beş tuzak merkezinin bulunduğunu gösterdi. Bu tuzak seviyelerinin yakalama kesit alanları ve tuzak yoğunlukları bu çalışmada sunuldu. Deneysel sonuçlar ile yavaş geri tuzaklanmaya dayalı teorik öngörülerin uyumlu olması bu tuzak seviyelerinde geri tuzaklanmanın ihmal edilebilir olduğunu gösterdi. Farklı ışınlama sıcaklıkları sonucunda elde edilen ısıluyarılmış akım ölçüm verilerinin analizi tuzak seviyelerinin üstel dağılımını ortaya çıkardı.

Emilme katsayısı ve kırılma indisini bulmak için 400-1100 nm dalgaboyu aralığında TlInS$_2$ kristalinin geçirgenlik ve yansıtıcılık spektrumları ölçüldü. Oda sıcaklığındaki emilme verilerinin analizleri, doğrudan ve dolaylı

geçişlerin bir arada bulunduğunu gösterdi. Sıcaklık 10K'den 300K'e arttıkça emilme kenarının daha düşük enerji değerlerine doğru değiştiği gözlemlendi. Ayrıca titreşim ve dağılma enerjileri ile sıfır frekans kırılma indisi belirtildi. Bunların yanı sıra, TlInS$_2$ kristalinin kimyasal bileşimi enerji dağılımlı spektrum analizi ile bulundu. Monoklinik birim hücre parametreleri x-ışını toz difraksiyon çalışması ile belirlendi.

Anahtar Kelimeler: Katmanlı Yarıiletkenler, Isıluyarılmış Akım, Elektriksel Özellikler, Safsızlıklar, X-ışını Kırınımı, Enerji Dağılımlı Spektrum Analizi, Fotogeçirgenlik, Optik Sabitler.

ACKNOWLEDGMENTS

To My Father

TABLE OF CONTENTS

LIST OF TABLES

TABLES

LIST OF FIGURES

FIGURES

CHAPTER 1

INTRODUCTION

The family of crystals designated with the chemical formula $TlBX_2$ (where B = In or Ga, X = S, Se or Te) are known as thallium dichalcogenides. Members of this family have both layered ($TlGaS_2$, $TlGaSe_2$, $TlInS_2$) and chain ($TlInSe_2$, $TlInTe_2$, $TlGaTe_2$) structures. They have become interesting due to their interesting structural properties and potential optoelectronic applications [1]. Their quasi-low dimensionality, optical and photoconductive properties and other features attract the attention of researchers to study these compounds.

At room temperature, the layered crystal $TlInS_2$ belongs to the monoclinic system with a space group C2/c and consists of a 1:1 ratio of InS:TlS. The lattice of $TlInS_2$ crystals consists of alternating two-dimensional layers parallel to the (001) plane with each successive layer turned through a right angle with respect to the preceding layer. A high photosensitivity in the visible range of spectra, high birefringences in conjunction with a wide transparency range of 0.5-14 μm make this crystal useful for optoelectronic applications [2,3]. For possible applications as an optoelectronic device in the visible range, a great deal of attention has been devoted to the study of the structural [1, 4-7], electrical [8-10] and optical [8,11-15] properties. These properties of semiconductors differ due to individual characteristics of energy gaps and impurities. The determination of activation energies of trapping centers in the energy gap takes an important role in the study of the properties of semiconductors.

1

Among many TlBX$_2$-type compounds, TlInS$_2$ has been studied rather well. The forbidden energy gap of TlInS$_2$ was measured by both absorption and reflection spectroscopy as a function of temperature and was found to be a direct band gap with an energy of 2.58 eV at T = 10 K [11,12]. Optical properties of TlInS$_2$ were also studied in Refs [8,16,17]. It was revealed the TlInS$_2$ crystals have two energy gaps, consisting of a direct and an indirect one, which were found to be equal to 2.23 and 2.28 eV at 300 K, respectively.

Photoluminescence (PL) spectra of TlInS$_2$ and their temperature and excitation intensity dependences in the 500-860 nm wavelength region have been reported in Ref. [18]. In this study, two PL bands centered at 515 nm (2.41 eV, A-band) and 816 nm (1.52 eV, B-band) at T = 11.5 K and excitation intensity of 7.24 W/cm^2 were observed. Analysis of the experimental data revealed that emission A-band was due to radiative transitions from shallow donor level located at 20 meV below the bottom of the conduction band to the moderately deep acceptor level located at 250 meV above the top of the valence band.

In Ref. [19], the temperature dependence of the optical energy gap of TlInS$_2$ crystal has been studied in the temperature range 77-300 K. After the analysis of the experimental data, the energy gap was found to be 2.24 eV at room temperature. Also the analysis of the dependence of the energy gap on temperature showed that the energy gap E_g was temperature dependent and the relation was linear in the temperature range from 77 to 300 K with a negative temperature coefficient dE_g/dT equal to 1.87 x 10^{-4} eV K^{-1}.

Dark electrical resistivity, photoconductivity and Hall measurements were studied to represent the donor energy levels in TlInS$_2$ single crystals in the temperature range of 100-400 K, 110-350 K, 170-400 K, respectively [20]. The donor energy levels located at 360, 280, 152 and 112 meV were found in the analysis of Hall coefficient and photocurrent measurements. The measurements of dark electrical resistivity and Hall coefficient also revealed that the conductivity type of TlInS$_2$ crystals changes at critical temperature T_c of 315 K from p-type to n-type.

Thermally stimulated currents (TSC) technique has been extensively used in the past to obtain information on the impurity and defect centers in the crystal, which was very useful in fabricating high-quality devices [21-25]. The study of processes in the TSC technique and methods to evaluate the electron trapping parameters picked up with the work of Randall and Wilkins in 1965 [26]. In this paper, their theoretical approach was based on the assumption that carriers, which are thermally excited from the trap levels, have a negligible probability of being retrapped. In 1960, Haering and Adams [27] presented another theoretical work which is an extension of the study of Randall and Wilkins. They studied the theory of thermally stimulated currents in the case of slow and fast retrapping. In 1964, Nicholas and Woods examined the electron trapping parameters from conductivity glow curves in CdS crystals by using the methods which have been proposed in the previous study [28]. Another theoretical paper was presented by Dussel and Bube in 1967. The study of this paper was based on the detailed theory of TSC for the case of a single type of trap and a single type of recombination centre [29].

There are only two papers in the literature in which TSC technique is used to determine the trapping parameters in $TlInS_2$ single crystals. Özdemir et al. [30] have investigated the trap levels in $TlInS_2$ crystals by TSC spectroscopy in the high-temperature range of 90-300 K. Analysis of the experimental spectra represented a series of trap levels with energy depths ranging from 150 to 220 meV in the energy gap. The shallow levels in the crystals in the temperature range below 90 K have been studied in Ref. [31]. In this study, the TSC measurements in $TlInS_2$ crystals over the temperature range of 10-90 K revealed that there was a trap level in the energy gap with activation energy of 12 meV. Also TSC measurements on quaternary semiconductor Tl_2InGaS_4, a structural analogue of $TlInS_2$, in which a half of indium atoms are replaced by gallium atoms, were carried out [32]. The activation energies of trapping centers were found to be equal to 4 and 10 meV. The capture cross section and concentration of the traps for Tl_2InGaS_4 crystals were also reported in this study.

The purpose of the present thesis is to concentrate mainly on the

3

experimental study of the trap distribution in undoped β-TlInS$_2$ layered crystals by using TSC measurements. Moreover, the TSC data is analyzed by using various methods. The activation energy, capture cross section, attempt to escape frequency and concentration of traps for all peaks observed in the TSC spectra of TlInS$_2$ crystals is determined. In addition to TSC measurements, results of the transmission and reflection measurements performed on the high quality TlInS$_2$ layered crystals are presented. Also, the results of the energy dispersive spectroscopic analysis and x-ray analysis in the 10-70° Bragg-angle (2θ) range will be used to determine the atomic composition ratio and lattice parameters of the TlInS$_2$ crystals, respectively.

CHAPTER 2

THEORETICAL APPROACH

2.1 Introduction

Materials that have electrical conductivity in between that of conductors and insulators are called semiconductors. Although they are normally insulators at low temperature, they can be conductors at a certain rate under the effect of light, heat and voltage. At the same time adding particular impurities to them can increase the conductivity of the semiconductors. The controllable conductivity properties of semiconductors make these materials attractive in many areas of the science. Modern electronic devices produced by semiconductor materials and instruments are very important in electronic device technology and they are used as an indispensable part of this area for the last forty years. Therefore, it is important and necessary to understand the fundamentals of semiconductors because of their increasing importance in technology.

The aim of this chapter is to give some information about the basic properties of semiconductors and thermally stimulated current technique used for the analysis of semiconductors.

2.2 Electronic Properties of Semiconductors

2.2.1 Band Structure

The difference of conductivity properties of conductor, insulator and semiconductor materials is mainly based on the different band structures of them. Although an atom has discrete energy levels, in semiconductors and insulators electrons are formed in a number of bands of energy. In the band structure of a solid, the highest energy band occupied by the electrons at absolute zero is called valence band. In semiconductors, the valence band is completely filled at low temperatures. The conduction band is the lowermost allowed energy band and is completely unoccupied by the electrons at absolute zero in semiconductors. The electrons in the conduction band can move freely throughout the solid. Thus, the conductivity of a material is proportional to the number of electrons in the conduction band. The band gap is defined as the energy difference between the valence and conduction bands. The band gap of a semiconductor material is less than that of insulator but higher than that of conductors. Figure 2.1 shows a simple model comparing the band gap of each type of material. The valence band electrons in semiconductors can be excited to the conduction band when they are given enough energy. The electrons excited to the conduction band increase the conductivity of the semiconductor material. This controllable conductivity property of the semiconductors has tremendously important role in many technological areas. The band gap of the semiconductors is less than 3 eV and insulators have higher band gap energy that is usually greater than 3 eV.
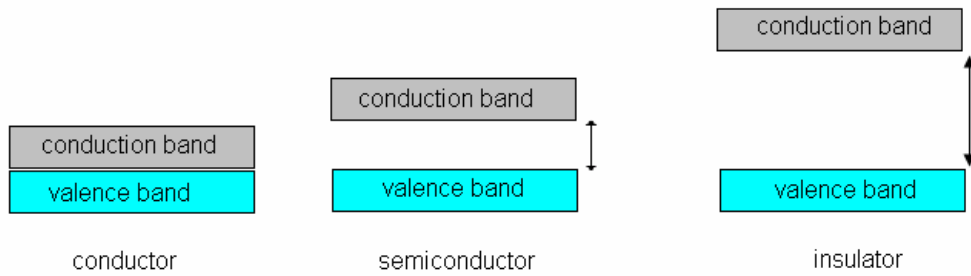
Figure 2.1. The relative comparison of band gap energies of conductors, insulators and semiconductors.

2.2.2 Intrinsic and Extrinsic Semiconductors

The most attractive property of the semiconductors is the controllable electrical conductivity. One of the methods to change their conductivity is to add some impurities. Semiconductors are divided into two types according to their purity called as intrinsic and extrinsic semiconductors. An intrinsic semiconductor, also called undoped semiconductor, is a pure semiconductor, which does not contain any impurity. This type of semiconductors does not display *n*- or *p*-type conductivity. The number of electrons in the conduction band and holes in the valence band are equal to each other (n = p). The density of charge carriers only depends on the properties of the material itself.

In some semiconductors, impurities are added mainly to change the electrical properties of these semiconductors. Such a semiconductor, which contains dopant atoms or impurities, is called an extrinsic semiconductor. The number of the charge carriers and conductivity of the semiconductor is determined by the added dopant elements.

2.2.3 Semiconductor Doping

Doping is the process in which impurities are intentionally added into the pure semiconductor. The purpose of semiconductor doping is to change the electron and hole number difference and by this way to increase the number of free charge carriers moving freely inside the solid by an external applied voltage. The type of the conductivity of the semiconductor depends on the added impurity atoms. If the impurity atoms have more valence electrons than that of host atoms, these valence electrons replace in the semiconductor lattice, this type of impurity is called as donor. Donor impurities donate additional electrons to the semiconductor's conduction band. Figure 2.2a shows a silicon (Si) crystal, having four valence electrons, doped with phosphorus (P) having five valence electrons. Four valence electrons of the phosphorus make covalent bonds with the corresponding four valence electrons of the silicon. The excess one electron can move around the crystal and increases the electron carrier concentration of the silicon. In this type of doping, the electrons become the majority charge carrier while holes become the minority charge carriers. This type of semiconductors is called n-type semiconductors. The donor level lies close to the conduction band in the energy gap (figure 2.3a).

On the other hand, if the impurity atoms have less valence electron than the atoms they replace in the semiconductor lattice, this kind of impurity is called as acceptor impurity. This lack of electron creates holes in the lattice. These holes increase the hole carrier concentration of the semiconductor and the holes become the majority charge carriers and electrons become the minority charge carriers. This type of semiconductors is called p-type semiconductors. Silicon doped with group III impurity atoms can be given as an example to this type of doping. When these impurity atoms are added to the pure Si crystal, one electron will be missing to complete the four covalent bonds. This is shown in the figure 2.2b. In such a case, the acceptor level lies close to the valence band in the energy gap (figure 2.3b).
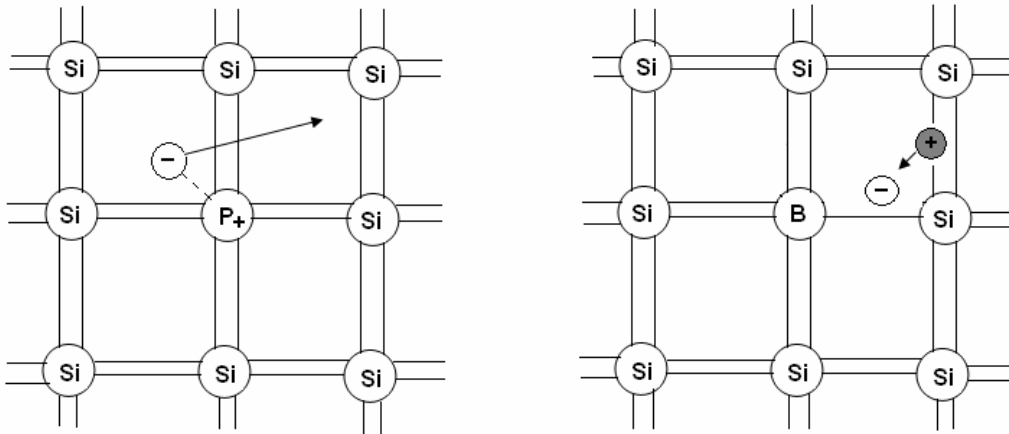
Figure 2.2. (a) a silicon (Si) crystal doped with phosphorus (P), (b) a silicon (Si) crystal doped with group III impurity atoms.

Conduction band	Conduction band
- - - - - - - - - Donor level	
	Acceptor level - - - - - - - -
Valence band	Valence band
(a)	(b)
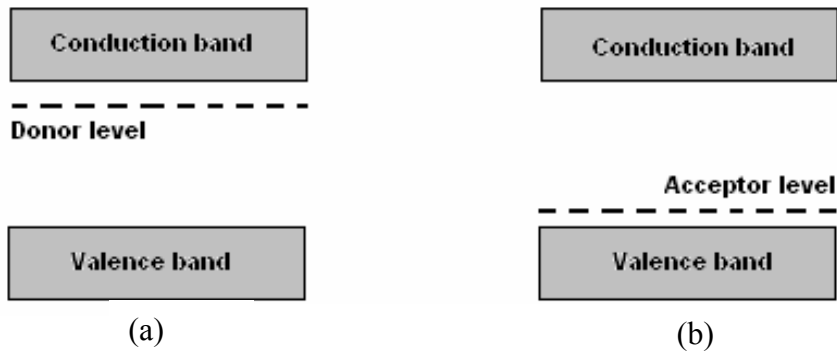
Figure 2.3. (a) The donor level, (b) acceptor level in a semiconductor.

2.2.4 Defects

The crystals in the nature are never perfect. All crystals have some defects or irregularities in their ideal arrangements. Although it seems that defects cause problems, these defects have an important role in the use of

materials in the semiconductor science and determine many properties of the materials.

There are mainly two types of crystal defects called as point defects and line defects-dislocations.

Point defects are the dimensionless defects where an atom is missing at one or more lattice locations or is in an irregular place in the lattice structure. There exist mainly four kinds of point defects in the crystal lattice. All these kinds of defects are shown in the figure 2.4.

(i)   Self interstitial atoms: These are the extra atoms which are the same type with the atom already present in the lattice and sit in an interstitial position.

(ii)   Interstitial impurity atoms: These are the atoms, which are smaller than the atoms in the crystal and fit into the open space between the bulk atoms of the lattice structure.

(iii)   Substitutional impurity atoms: These are the different type of atoms in the lattice structure instead of the bulk atom.

(iv)   Vacancies: Vacancies exist when an atom is missing at one or more lattice sites. These missing atoms leave an empty region in its place.

(i)   (ii)   (iii)   (iv)
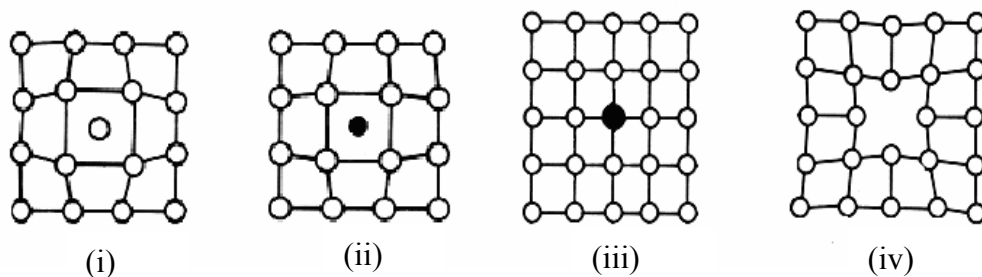
Figure 2.4. (i) Self interstitial atom, (ii) Interstitial impurity atom, (iii) Substitutional impurity atom, (iv) Vacancy.

In the line defects, groups of atoms are in irregular positions. Line defects are also called dislocations. There are two types of dislocations:

(a) Edge dislocation: This dislocation exists when an extra half-plane of atoms is replaced in or removed from the crystal structure (figure 2.5a)

(b) Screw dislocation: If the dislocation is formed by the displacement of atoms in a plane in the crystal then a screw dislocation is observed. A step or ramp is formed in this type of dislocation (figure 2.5b).
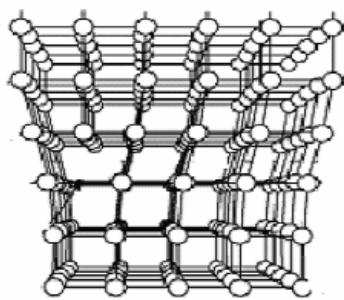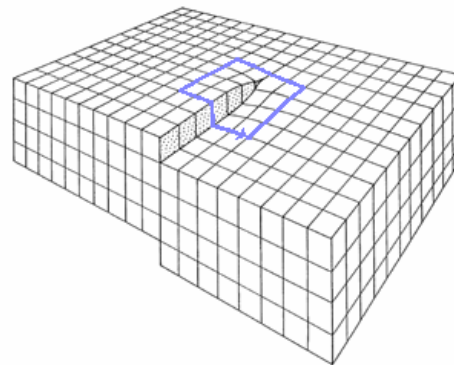
(a)   (b)

Figure 2.5. (a) Edge dislocation; (b) Screw dislocation [33].

2.3 X-ray Diffraction Experiments

X-rays are electromagnetic waves with a wavelength in the range of 10^{-8} to 10^{-11} m and this wavelength is of the same order of magnitude with the spacing between the planes of crystal. Thus x-rays are used to produce diffraction pattern. X-ray diffraction experiments are utilized to obtain information about the interplanar spacing between planes of atoms, the crystal structure of an unknown material and the orientation of a crystal.

The theoretical explanation of x-ray diffraction experiment is as follows: X-rays are radiated onto a material, which consists in crystals with a spacing d between its planes (figure 2.6). These x-rays will be reflected after colliding with the electrons in the crystal lattice. According to the law of reflection, the angle of incident light θ will be equal to the angle of reflection. The reflection of x-rays from different atoms causes a path difference between them. The path difference between any two successive rays is equal to

$$|AB| + |AC| = 2d \sin \theta. \tag{2.1}$$
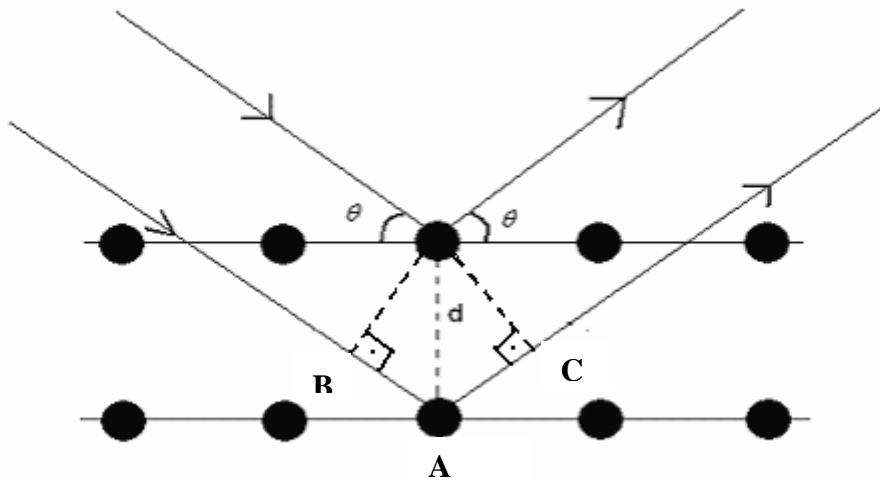
Figure2.6. Representation of x-ray diffraction by a crystal lattice.

X-rays scattered from different electrons constitute constructive or destructive interference due to their path differences. If the path difference between any two rays is an integer multiple of the wavelength (λ) of emitted x-rays, these rays interfere constructively. The mathematical relation of this constructive interference is called "Bragg's law" and given by the expression [34]

$$2d_{hkl} \sin\theta = n\lambda \;, \qquad n = 0,1,2,3.... \qquad\qquad (2.2)$$

where n is an integer.

The interplanar spacing d depends only on the type and size of the unit cell and Miller indices. Bragg's law and expression to find the d from the Miller indices can be combined for different kind of crystals to determine the lattice parameters. The interplanar spacing d as a general form is given by the expression

$$\frac{1}{d_{hkl}^2} = \frac{1}{\left[1 + 2\cos(\alpha)\cos(\beta)\cos(\gamma) - \cos^2(\alpha) - \cos^2(\beta) - \cos^2(\gamma) \right]}$$
$$\times \left[\frac{h^2 \sin^2(\alpha)}{a^2} + \frac{k^2 \sin^2(\beta)}{b^2} + \frac{l^2 \sin^2(\gamma)}{c^2} \right.$$
$$+ \frac{2hk}{ab}(\cos(\alpha)\cos(\beta) - \cos(\gamma)) + \frac{2kl}{bc}(\cos(\beta)\cos(\gamma) - \cos(\alpha))$$
$$\left. + \frac{2lh}{ac}(\cos(\gamma)\cos(\alpha) - \cos(\beta)) \right] \;, \qquad\qquad (2.3)$$

where a, b and c are lattice constants, h, k and l are Miller indices and α, β and γ are the angles for the lattice structure.

2.4 Energy Dispersive Spectral Analysis Experiments

Energy dispersive spectral analysis (EDSA) also called energy dispersive x-ray analysis (EDXA) is an analytical method used to get information about the chemical characterization of any sample. As a spectroscopy technique, EDSA mainly depends on the interaction between electromagnetic radiation and sample. The basic physical principle of EDSA technique is described as follows:

13

When a sample is bombarded with a particle beam such as electron beam, the ground state electrons within the atom are excited to an inner shell. The excited electron leaves a hole within the atom's electronic structure. Then an outer shell electron fills this hole by exposing energy. The excess energy of this transmission is emitted as x-ray from the atom. The fundamental principle in EDSA is that every element has a unique atomic structure and this uniqueness allows the emitted x-rays being the characteristic of an element's atomic structure. Thus, the x-rays emitted by the sample are analyzed to understand the chemical properties of the sample. In addition to knowing the composite elements in a material, EDSA analysis is also used to determine the ratio of each element in the material.

2.5 Optical Absorption, Transmission and Reflection of Semiconductors

Absorption, transmission and reflection experiments are simple methods for evaluating some optical properties of semiconductors. The analysis of such measurements mainly based on the relation between the intensity of incident, transmitted and reflected light.

(i) **Absorption**: When a light is radiated on a semiconductor, some of them are absorbed through the material if the energy of the light is equal or higher than the band gap energy of the solid. In the absorption process, an electron in the lower energy state is excited to a higher energy state by absorbing the energy of the incident light. The intensity of the incident light decreases after the absorption process. Then the fraction of intensity of the incident light after propagation a distance x through the material is given by [35]

$$\frac{I(x)}{I_0} = \exp(-\alpha x) \ , \tag{2.4}$$

where I_0 is the intensity of the incident light, $I(x)$ is the intensity after this propagation and α is the absorption coefficient defined as

$$\alpha = \frac{4\pi k}{\lambda} \ ,$$
(2.5)

where λ is the wavelength of the light wave and k is the absorption index of the material.

The absorption coefficient, α, for a given photon energy $h\nu$ depends on the probability of the transition from the initial state to final state. The absorption coefficient α, photon energy $h\nu$ and band gap energy E_g are related by the expression [36]

$$(\alpha h\nu) = A(h\nu - E_g)^{\text{p}} \ ,$$
(2.6)

where A is constant which depends on the transition probability and p is an index characterizing the optical absorption process. The value of the p is equal to 2 and 1/2 for indirect and direct allowed transitions, respectively.

(ii)   **Reflection**: When the light is sent to the material, some of them is reemitted by the material to the incoming plane. This process is called reflection and for normal incidence, the reflection coefficient is given by [35]

$$R = \frac{(n-1)^2 + k^2}{(n+1)^2 + k^2} \ ,$$
(2.7)

where n is the refractive index of the material. In the transparent range in which absorption index k is equal to zero, the reflection coefficient becomes

15

$$R = \frac{(n-1)^2}{(n+1)^2} \ .$$ (2.8)

(iii) **Transmission**: When the light normally falls on the material, some of them propagate through the material and then leaves the material without changing its direction. This process is called as transmission. The transmission coefficient is defined as the ratio of the intensities of transmitted and incident light and given by [35]

$$T = \frac{(1-R)^2 \exp(-\alpha x)}{1 - R^2 \exp(-2\alpha x)} \ ,$$ (2.9)

where x is the thickness of the material. When the product αx is large, then $\exp(-2\alpha x) \approx 0$ and transmission coefficient is equal to

$$T \cong (1-R)^2 \exp(-\alpha x) .$$ (2.10)

If R and x are known, α can be evaluated from the equation 2.9. If the refractive index n is known, the thickness of the thin sample can be obtained from the transmission interference fringes at wavelengths slightly longer than the absorption edge. The expression describing thickness from this method is

$$x = \frac{1}{2n}\left(\frac{\lambda_1 \lambda_2}{\lambda_1 - \lambda_2}\right) \ ,$$ (2.11)

where λ_1 and λ_2 are the positions of the two neighboring peaks.

Moreover, the dispersive refractive index data for $h\nu < E_g$ can be analyzed according to the single-effective-oscillator model proposed by Wemple and DiDomenico [37,38]. In this model, the refractive index is related to photon energy through the relation

16

$$n^2 = 1 + \frac{E_{so}E_d}{E_{so}^2 - (h\nu)^2} \quad , \quad\quad\quad (2.12)$$

where E_{so} is the single oscillator energy and E_d is the dispersion energy. E_{so} and E_d parameters are evaluated from the graph of $(n^2 - 1)^{-1}$ versus $(h\nu)^2$ by fitting a linear function to the lower energy range. Also the zero-frequency refractive index n_0 is obtained from the equation 2.12 by replacing $h\nu = 0$. The expression for n_0 is obtained as

$$n_0^2 = 1 + \frac{E_d}{E_{so}} \quad . \quad\quad\quad (2.13)$$

2.6 Thermally Stimulated Processes

Thermally stimulated processes cover a number of some physical techniques in which the sample is heated and a property of the sample is measured as a function of temperature. The result of such a measurement is a curve of measured parameter as a function of temperature or time. The analysis of this curve is used in many areas of physics and chemistry to determine various properties of materials. The most important thermally stimulated processes are [24]:

(i)   Thermoluminescence.
(ii)   Thermally stimulated current.
(iii) Thermally stimulated electron emission.
(iv)   Deep level transient spectroscopy.
(v)   Thermally stimulated depolarization currents.

2.7 Thermally Stimulated Current

2.7.1 Transitions in the Thermally Stimulated Current Process

The thermally stimulated current (TSC) technique is extensively used to get information on the impurity and defect centers in the crystal. In this method, the sample excited previously at an initial low temperature is heated under the voltage applied across the contacts connected to the sample. While heating the sample linearly, the transient electric currents in the sample are measured as a function of the temperature. The resulting curve is called a TSC curve and usually in the form of peak(s), giving information about the properties of shallow and/or deep trapping levels within the band gap.

The possible transitions of electrons in the band gap are the main physical events considered in the TSC experiments. The major electronic transitions associated with the TSC are described below and represented in the figure 2.7.
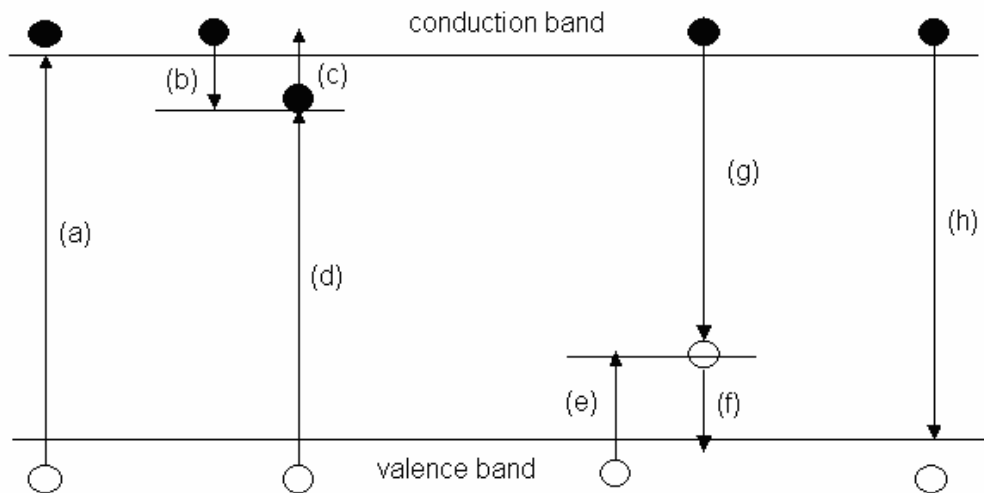
Figure 2.7. Possible electronic transitions in the TSC technique. (a) band-to-band excitation; (b) and (e) electron and hole trapping, respectively; (c) and (f) electron and hole release; (d) and (g) indirect recombination; (h) direct recombination. Solid circles, open circles and arrows represent electrons, holes and transitions, respectively [39].

(I)   Transition (a) is the band-to-band excitation of a valence band electron to conduction band. This transition occurs when valence band electron is given enough energy from an external source.

(II)   Transitions (b) and (e) are called as electron and hole trapping, respectively. Excited electrons and holes in the conduction and valence bands will return to their initial band. Through this return some of the electrons and holes are trapped at trapping centers.

(III) Transitions (c) and (f) are called as electron and hole releases. When enough energy is given to electrons and holes in the trapping centers, they are excited to conduction or valence bands, respectively.

(IV) Transitions (g) and (d) are indirect recombination mechanisms. These transitions occur when free electrons and holes in the conduction and valence bands, respectively, recombine with a charge carrier of opposite sign in the trapping centers.

(V)   Transition (h) is the direct recombination defined as the recombining of a charge carrier in the conduction band with an opposite sign charge carrier in the valence band.

The following simple model can explain the TSC method: The electrons are excited by some kind of radiation from the valence band to the conduction band at an initial low temperature (transition a). Most of the electrons in the conduction band return to the ground state in a short time (transition h). Some of them are trapped in the trapping centers associated with the lattice defects such as vacancies, interstitials or impurities (transition b). A hole is created in the valence band in the place of electron trapped in the trapping center. These holes are also trapped in the hole trap centers (transition e). These trap electrons (holes) return back to conduction (valence) band when a sufficient energy is given (transitions c and f). In the thermally stimulated processes the type of the given energy is thermal energy. The electrons excited to the conduction band give a transient increase in the conductivity of the sample. This increase is observed as a peak in the TSC curve of the sample. The analyses of the peak(s)

19

give information about the some properties of the trap levels such as activation energy and concentration of electrons in these centers.

2.7.2 Theoretical Approach

At a temperature T, the probability P that an electron can be released back into the conduction band from a trap depth of E (transition c) is given by

$$P = \nu \exp(-E/kT),\qquad(2.14)$$

where ν is the attempt-to-escape frequency and k is the Boltzmann constant. In a semiconductor, ν is defined by the expression

$$\nu = N_c\, \upsilon_e\, S_t,\qquad(2.15)$$

where S_t is the capture cross section, N_c and υ_e are the effective density of states in the conduction band and thermal velocity of the conduction electrons, respectively. N_c and υ_e are given by

$$N_c(T) = 2(\frac{kTm_e^*}{2\pi\eta^2})^{2/3}\qquad(2.16)$$

and

$$\upsilon_e(T) = \sqrt{\frac{3kT}{m_e^*}}\quad,\qquad(2.17)$$

where m_e^* is the electron effective mass.

The concentration of filled traps (n) mainly depends on the transitions from or to trapping center. These possible transitions and their theoretical explanations are [24]:

(i)   Stimulation (transition c): The transition from the trapping center to the conduction band affects the concentration of filled traps. Decrease of trapped electron population is dependent on the concentration n and given by the relation

$$\frac{dn}{dt} \propto -n\,v\exp(-E/kT)\cdot$$
(2.18)

(ii)   Retrapping: In addition to the excitation transition we should also take into account the retrapping (transition b). The probability of retrapping process depends on both the concentration of free electrons n_c in the conduction band and the concentration of unoccupied traps $(N-n)$, where N is the total concentration of traps. The relation describing the effect of retrapping on the rate of change of trapped electron concentration is

$$\frac{dn}{dt} \propto n_c(N-n)S_t v_e\cdot$$
(2.19)

The total rate of change of electron concentration can be obtained as

$$\frac{dn}{dt} = n_c(N-n)S_t v_e - n\,v\exp(-E/kT)\,.$$
(2.20)

by combining equations 2.18 and 2.19.

An electron excited to the conduction band can either be trapped or recombine with a hole, directly or through a recombination center. The rate of the recombination is n_c/τ, where τ is defined as recombination lifetime [40]. Then the rate of change of the free electrons concentration n_c is equal to

21

$$\frac{dn_c}{dt} = -\frac{n_c}{\tau} - \frac{dn}{dt} \quad . \tag{2.21}$$

For the solution of equations 2.20 and 2.21, two fundamental assumptions have been suggested.

(1) **Slow Retrapping**: As suggested by Randall and Wilkins [26], in this case the retrapping of a charge carrier is negligible compared to the rate of recombination and the electron released to the conduction band recombines quickly with a hole. This assumption also called as "first order kinetics" is expressed by the following inequalities:

$$\frac{n_c}{\tau} \gg n_c (N - n) S_t \upsilon_e \tag{2.22}$$

and

$$\left| \frac{dn_c}{dt} \right| \ll \left| \frac{dn}{dt} \right| \quad . \tag{2.23}$$

Using equations 2.22 and 2.23, equation 2.20 becomes

$$\frac{dn}{dt} \approx -n \, \nu \exp(-E/kT), \tag{2.24}$$

and

$$\frac{dn}{dt} \approx -\frac{n_c}{\tau} \quad . \tag{2.25}$$

Integrating equation 2.24 by assuming a linear heating function $T = T_0 + \beta t$, we get

$$n = n_0 \exp\left\{-\int_{T_0}^{T} \frac{\nu}{\beta} \exp(-E/kT)\, dT\right\} , \qquad (2.26)$$

where n_0 is the initial trapped electron concentration at initial temperature T_0. Then substituting equations 2.25 and 2.26 into equations 2.24, we get

$$n_c = n_0 \tau \nu \exp\left\{-\frac{E}{kT} - \int_{T_0}^{T} \frac{\nu}{\beta} \exp(-E/kT)\, dT\right\} , \qquad (2.27)$$

the thermally stimulated conductivity σ is given by

$$\sigma = n_c e\mu = n_0 \tau \nu e\mu \exp\left\{-\frac{E}{kT} - \int_{T_0}^{T} \frac{\nu}{\beta} \exp(-E/kT)\, dT\right\} , \qquad (2.28)$$

where τ is the lifetime of a free electron, μ is the electron mobility, β is the heating rate and T_0 is the initial temperature. Then the thermally stimulated current is described by the equation

$$I = n_0 \tau \nu e\mu \left(\frac{V}{L}\right) A \exp\left\{-\frac{E}{kT} - \int_{T_0}^{T} \frac{\nu}{\beta} \exp(-E/kT)\, dT\right\} , \qquad (2.28a)$$

where V is the applied voltage, A and L are the area and length of the sample.

(2) **Fast Retrapping**: Haering and Adams (1960) considered the case in which the time required for thermal equilibrium between the conduction electrons and trapped electrons is much shorter than the recombination lifetime [27]. If we show the total number of electrons by

$$n_t = n + n_c, \qquad (2.29)$$

and assume

$$N \gg N_c \exp(-E/kT) \qquad (2.30)$$

for fast trapping process, then the rate of change of total electrons is

$$\frac{dn_t}{dt} = -\frac{n_c}{\tau} = -\frac{n_t}{\tau}\left(\frac{N_c}{N}\right)\exp\left(-\frac{E}{kT}\right), \qquad (2.31)$$

where n and n_c are concentration of electrons in traps and conduction band, N and N_c are concentration and effective concentration of trapping and conduction states, respectively, and τ is the recombination lifetime. The solution of the equation 2.31 is

$$n = n_0 \exp\left[-\frac{1}{\beta}\int_{T_0}^{T}\frac{N_c}{N\tau}\exp(-E/kT)dT\right] \qquad (2.32)$$

and the thermally stimulated current is

$$I = \left(\frac{V}{L}\right)A\frac{N_c\mu}{N}en_0 \exp\left[-\frac{E}{kT} - \frac{N_c}{N\beta\tau}\int_{T_0}^{T}\exp(-E/kT)\,dT\right]. \qquad (2.33)$$

2.7.3 Curve Fitting

(i) Slow Retrapping: The TSC curve of traps for the first order kinetics is described by the equation 2.28a. If it is assumed that ν is independent of

temperature T and the variation of μ and τ is negligible with temperature range of TSC experiment, equation 2.28a can be rewritten as [41]

$$I = \left(\left(\frac{V}{L} \right) A \right) A_0 \exp \left\{ -t + B' \int_{t_0}^{t} \exp(-t) t^{-2} dt \right\} , \qquad (2.34)$$

where $t = \dfrac{E}{kT}$ and, A_0 and B' are constants:

$$A_0 = n_0 \tau e \mu v \qquad \text{and} \qquad B' = \frac{v E_t}{\beta k} , \qquad (2.35)$$

where n_0 is the initial density of traps. If repeated integration by parts of integral in equation 2.34 is taken, we get a convergent infinite series expression;

$$I = \left(\left(\frac{V}{L} \right) A \right) A_0 \exp \left[-t - B' \left\{ \exp(-t) t^{-2} - 2 \exp(-t) t^{-3} + 3 \times 2 \exp(-t) t^{-4} \ldots \right\}_{t_0}^{t} \right] .$$

$$(2.36)$$

Because t is large in practice, by making approximation, the infinite series can be written as

$$I \approx \left(\left(\frac{V}{L} \right) A \right) A_0 \exp \left[-t - B' \exp(-t) t^{-2} \right] , \qquad (2.37)$$

$$I \approx I_0 + \left(\left(\frac{V}{L} \right) A \right) A_0 \exp \left[-t - B' \exp(-t) t^{-2} \right] , \qquad (2.38)$$

where I_0 is the value at t_0. If equation 2.38 is differentiated and equated to zero to find the maximum of the curve, which occurs at

$$t = t_m = \frac{E_t}{kT_m}, \tag{2.39}$$

then

$$B' = \exp(t_m)\frac{t_m^3}{t_m + 2} . \tag{2.40}$$

(ii) Fast Retrapping: In the equation 2.33 for second order kinetics given by Haering and Adams, if we insert $t = \dfrac{E}{kT}$, it becomes [42]

$$I = \left(\frac{V}{L}\right)AC\exp\left[-t + D\int_{t_0}^{t}\exp(-t)t^{-7/2}dt\right], \tag{2.41}$$

where

$$C = \frac{N_c e\mu n_0}{N} \quad \text{and} \quad D = \frac{N_c E^{5/2}}{N\beta T^{*3/2}k^{5/2}\tau} . \tag{2.42}$$

Repeated integration by parts of equation 2.41, and then approximation gives

$$I \approx C\exp\left[-t - D\exp(-t)t^{-7/2}\right] . \tag{2.43}$$

If equation 2.43 is differentiated and equated to zero to find the value of t^* at the maximum, D^* is found as

$$D^* = \frac{\exp(t^*)t^{*9/2}}{t^* + 3.5} . \tag{2.44}$$

where D^* is the value of D to the limits of the approximation used.

26

In order to analyze the peaks simultaneously, the fitting function is given by the sum

$$I(T) = \sum_{i=1}^{n} I_i(T) \ , \tag{2.45}$$

where $I_i(T)$ denotes the current contribution of each peak calculated by means of equation 2.38 or 2.43 for slow and fast retrapping, respectively, and n denotes the number of traps involved in the calculation.

Once the TSC curve have been fitted and the values E_t and T_m for peaks determined, equations 2.40 or 2.44 can be used to calculate B' or D^* for slow and fast retrapping processes, respectively. Also for the first order kinetics, the attempt-to-escape frequency ν can be calculated by using equation 2.35. Then the cross section of the traps was calculated using the value of ν and the following expression

$$S_t = \frac{\nu}{N_c \upsilon_{th}} \ , \tag{2.46}$$

where N_c is the effective density of states in the conduction band and υ_{th} is thermal velocity of a free electron.

The concentration of the traps was estimated using the relation [43]

$$N_t = \frac{Q}{ALeG} \ . \tag{2.47}$$

Here, Q is the quantity of charge released during a TSC experiment and can be calculated from the area under the TSC peaks; e is the electronic charge and G is the photoconductivity gain, which equals to the number of electrons passing

27

through the sample for each absorbed photon. The photoconductivity gain G was calculated from [25]

$$G = \frac{\tau}{t_{tr}} = \frac{\tau \mu V}{L^2} \ , \tag{2.48}$$

where τ is the carrier lifetime, t_{tr} is the carrier transit time between the electrodes and μ is the carrier mobility.

2.7.4 Initial Rise Method

Garlick and Gibson [28] first presented this method in 1948. Because initial rise method is independent of the recombination kinetics, it is an attractive method in the analysis of the TSC curves. The integrals in the first and second order equations 2.28a and 2.33 are very small when the traps begin to empty as the temperature is increased. Therefore, exponential terms in these integrals are very close to unity in this temperature range of the process. So the current is written as

$$I = C \exp(-E_t / kT) \ , \tag{2.49}$$

where C is constant. When the initial portion of the TSC curve is analyzed, the plot of ln (I) as a function of $1/T$ gives a straight line with a slope of ($-E_t/k$). The limitation of this method is that there must be no overlap peak in the initial rise portion of the analyzed peak.

2.7.5 Peak Shape Method

In the peak shape method, the activation energy of trap is associated by using three parameters (figure 2.8): $\tau = T_m - T_l$, $\delta = T_h - T_m$, $w = T_h - T_l$, where T_m is the temperature corresponding to the maximum current, T_l and T_h are the low and high half-intensity temperatures, respectively [24].
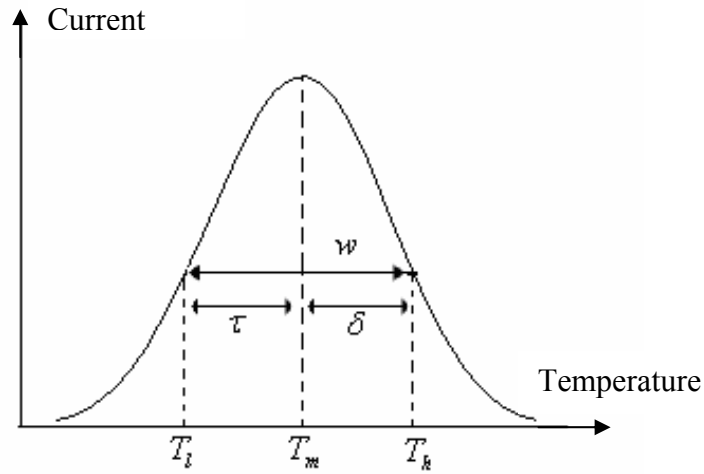
Figure 2.8. Representation of parameters used in peak shape method.

The activation energy of the trap is obtained by

$$E_\tau = \left[1.51 + 3.0(\mu_g - 0.42)\right]kT_m^2 / \tau - \left[1.58 + 4.2(\mu_g - 0.42)\right]2kT_m \qquad (2.50)$$

$$E_\delta = \left[0.976 + 7.3(\mu_g - 0.42)\right]kT_m^2 / \delta \qquad (2.51)$$

$$E_w = \left[2.52 + 10.2(\mu_g - 0.42)\right]kT_m^2 / w - 2kT_m , \qquad (2.52)$$

29

where μ_g is equal to ratio δ/w. In 1960 Halperin and Braner suggested to use μ_g value to understand the order of kinetics. The values of μ_g were predicted by Chen and Kirsh [24] as 0.42 and 0.52 for first and second-order kinetics, respectively. The peak shape method cannot be carried out on the curve, which contains more than one peak. If such a curve occurs, the analyzed peak can be cleaned from the other satellite peaks.

2.7.6 Isothermal Decay Method

This method is based on the shape of the decay curve with time. The procedure of the method is as follows: The sample is heated and then it is held at a constant temperature T_p. The thermally stimulated current can be described for this process by [24]

$$I = I_0 \exp(-\gamma t) \tag{2.53}$$

where I_0 is the initial current at time $t=0$ and

$$\gamma = \nu \exp(-E_t / kT_p). \tag{2.54}$$

Then the measurement is repeated at different values of temperature T_p and for all measurements, γ values are evaluated from the slopes of the plots ln (I) versus time t graph. The ln values of the slopes can now be plotted as a function of $1/T$ and a straight line with a slope of $(-E_t/k)$ is obtained.

2.7.7 Traps Distribution

Most analysis of the thermally stimulated current mentioned above are based on the assumption that the traps which are related to a specific defect have the same, discrete activation energy. However this assumption is not acceptable for all crystals. Especially in amorphous semiconductors it is observed that the band gap of these semiconductors contains a finite density of available states. Mott and Davies (1979) explained this picture by the assumption of the presence of localized states.

For the study of the traps distribution, we assume an exponential distribution of traps whose density at energy E is expressed by [44]

$$N(E) = A \exp(-\alpha E), \tag{2.55}$$

where α is the energy parameter which characterizes the distribution. Then, for this exponential distribution, we can write for the traps filled at the excitation temperature T_e

$$n_0(T_e) = A \exp(-\alpha E) \exp[(E - E_f)/kT_e], \tag{2.56}$$

where E is the Fermi level energy in darkness and E_f is the energy of the quasi-Fermi level for electrons during light excitation. E and E_f are written as

$$E = kT_m \ln[N_c/n_m] \quad (2.57) \qquad \text{and} \qquad E_f = kT_m \ln[N_c/n_e], \quad (2.58)$$

where n_m and n_e are the densities of free electrons at temperature T_m in darkness and during light excitation, respectively. n_0 is proportional to the area of the TSC curve, so equation 2.57 becomes

$$S_0(I_m / I_e) \propto A\exp(-\alpha E),\qquad\qquad (2.59)$$

where I_m and I_e are the currents flowing in the crystal at the peak temperature, in darkness and during light excitation, respectively.

CHAPTER 3

EXPERIMENTAL DETAILS

3.1 Introduction

Energy dispersive spectral analysis, x-ray diffraction analysis, transmission, reflection, thermally stimulated current and photoconductivity decay measurements were carried out on β-TlInS$_2$ crystals, which were synthesized from high-purity elements prepared in stoichiometric proportions. Single crystals were grown by the Bridgman method. The resulting ingot appeared orange in color and the freshly cleaved surfaces were mirror-like.

3.2 Energy Dispersive Spectral Analysis and X-ray Diffraction Experiments

The chemical composition of TlInS$_2$ crystal was determined by means of an energy dispersive spectroscopic analysis (EDSA) with a JSM-6400 scanning electron microscope. The equipments of the device, "NORAN System6 X-ray Microanalysis System" and "Semafore Digitizer", were used for the analysis of the experimental data.

X-ray diffraction technique was used to obtain information about the structural parameters of the samples. A "Rigaku Miniflex" diffractometer with CuKα radiation ($\lambda = 0.154049$ nm) were used at a scanning speed of 0.02°/sec

for the x-ray powder diffraction experiments. The crystal system, the Miller indices of the diffraction peaks and the lattice parameters were evaluated by using a least-squares computer program "DICVOL 04".

3.3 Transmission and Reflection Measurements

Transmission and reflection measurements were performed in the 400-1100 nm wavelength region by using a "Shimadzu" UV 1201 model spectrophotometer, which consisted of a 20 W halogen lamp, a holographic grating and a silicon photodiode. The resolution of the spectrophotometer was 5 nm. Transmission measurements were done under normal incidence of light with a polarization direction along the (001) plane, which is perpendicular to the *c*-axis of the crystal. For the room temperature reflection experiments, a specular reflectance measurement attachment with a 5° incident angle was used. Transmission and reflection measurements were performed in the temperature range 10-300 K. The sample was cooled from room temperature down to 10 K, within an accuracy of $\pm$ 0.5 K, by using an "Advanced Research Systems, Model CSW-202" closed cycle helium cryostat.

3.4 Thermally Stimulated Current Experiments

In a TSC experiment, traps are filled by band-to-band excitation of carriers at low temperatures using a suitable light source. These charge carriers remain in the trap centers until a sufficient amount of thermal energy is given to excite them to the conduction (valence) band. When these charge carriers are thermally excited to the conduction (valence) band upon heating, they give rise to a transient increase in the conductivity of the sample. The heating rate is usually desired to be constant for the sake of convenience in the analysis of the TSC peak(s).

For TSC measurements a sample with dimensions of 6.0 × 2.0 × 1.5 mm^3 were used. Electrical contacts were made on the sample surface with silver paste according to sandwich geometry. In the sandwich configuration, one of the electrodes is placed on the front surface of the crystal with a small droplet of silver paste. Then the sample is mounted on the sample holder with conducting silver paste. The second electrode is connected to the cryostat for circuit connection. The electrons flow through the crystal in the direction of parallel to the *c*-axis in the sandwich geometry. The simple schematic diagram of the sandwich geometry is shown in the figure 3.1. The electrical conductivity of the studied sample was n-type.
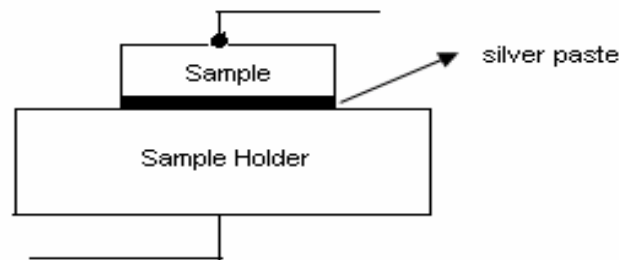
Figure 3.1. The simple presentation of the sample with sandwich configuration.

The TSC measurements were performed in the temperature range from 10 to 300 K using an Advanced Research Systems closed-cycle helium cryostat. Constant heating rates in the range of 0.2–1.5 K/s were achieved by a Lake-Shore 331 temperature controller. A Keithley 228A voltage/current source and a Keithley 6485 picoammeter were used for the TSC measurements. The temperature and current sensitivities of the system were about 10 mK and 2 pA,

35

respectively. The view of the TSC experimental set up is shown in the figure 3.2.
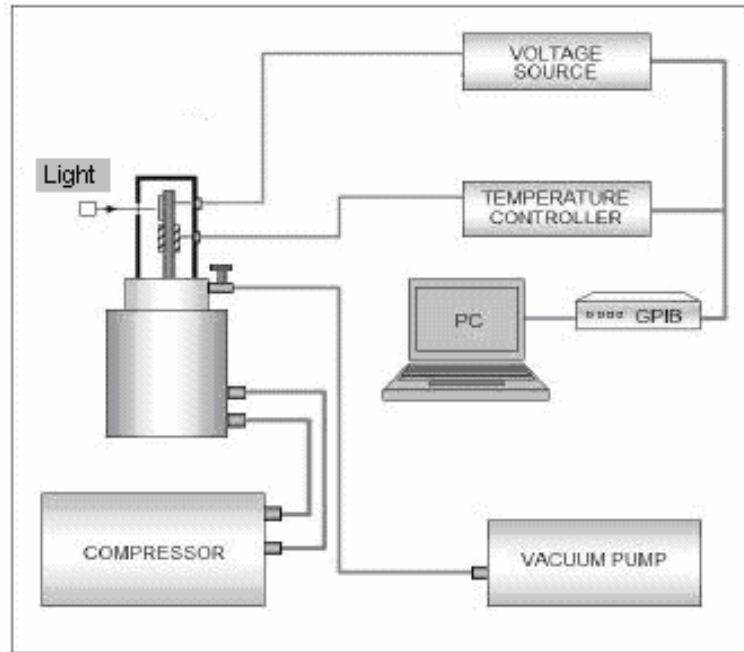
Figure 3.2. The diagram of the TSC experimental set up [45].

At low enough temperatures, when the probability of thermal release is negligible, the carriers are photo-excited by using a light emitting diode generating light at a maximum peak of 2.6 eV. When the excitation is turned off and an expectation time has elapsed, the DC field is applied to the sample and the temperature is increased at a constant rate. The TSC is obtained from the current in excess of the equilibrium dark current contribution.

The details of illumination time, voltage and initial temperature for TSC measurements of TlInS$_2$ crystal are shown in the figure 3.3 and 3.4.
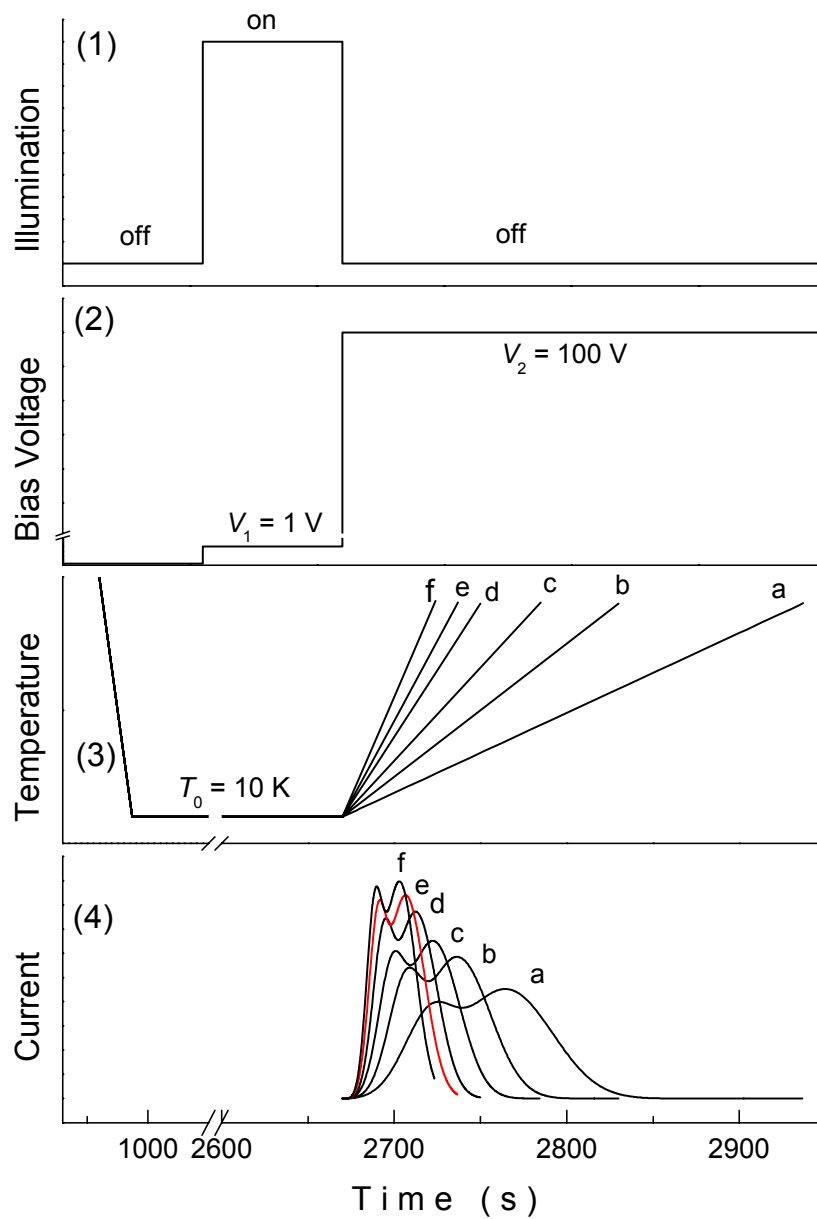
Figure 3.3. Experimental conditions of TSC measurements of TlInS$_2$ crystal in low temperature range. (1) time period of applied illumination; (2) variation of bias voltage; (3) temperature variation with time; (4) TSC peaks for different heating rates: 0.3 (a), 0.5 (b), 0.7 (c), 1.0 (d), 1.2 (e), 1.5 K/s (f).
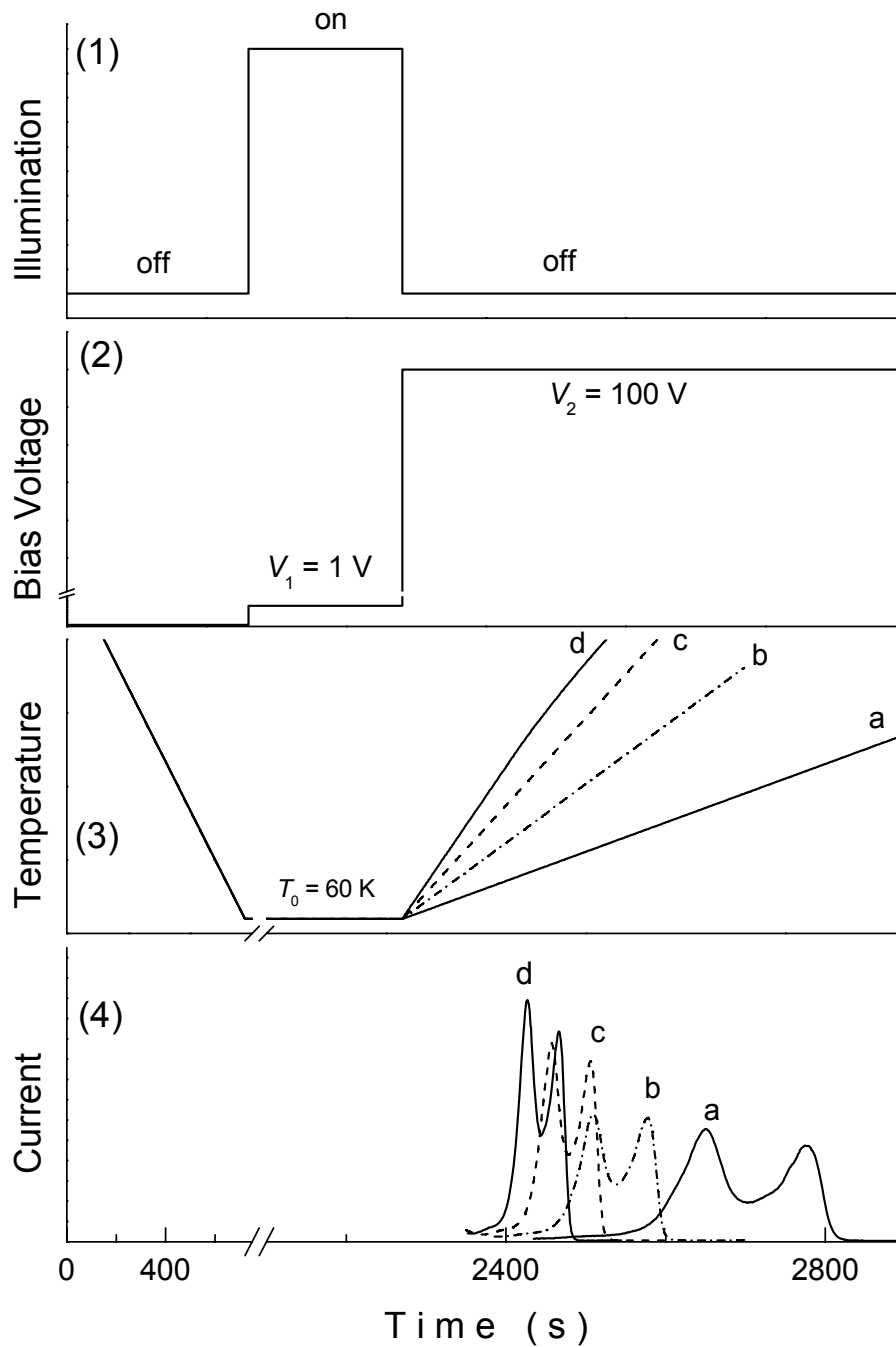
Figure 3.4. Experimental conditions of TSC measurements of TlInS$_2$ crystal in high temperature range. (1) time period of applied illumination; (2) variation of bias voltage; (3) temperature variation with time; (4) TSC peaks for different heating rates: 0.2 (a), 0.4 (b), 0.6 (c), 0.8 K/s (d).

3.5 Photoconductivity Decay Experiments

The carrier lifetime was determined from the photoconductivity decay experiments. In these experiments, two electrodes are attached to opposite surfaces of the TlInS$_2$ with silver paste. Then one of the contacts was illuminated by a high efficiency short-pulsed LED controlled by "NI USB-6211 high-performance USB data acquisition device". The signal was transmitted to the computer and then analyzed to determine the decay time of the photocurrent. The schematic block diagram of the photoconductivity decay experimental set up is shown in the figure 3.5.
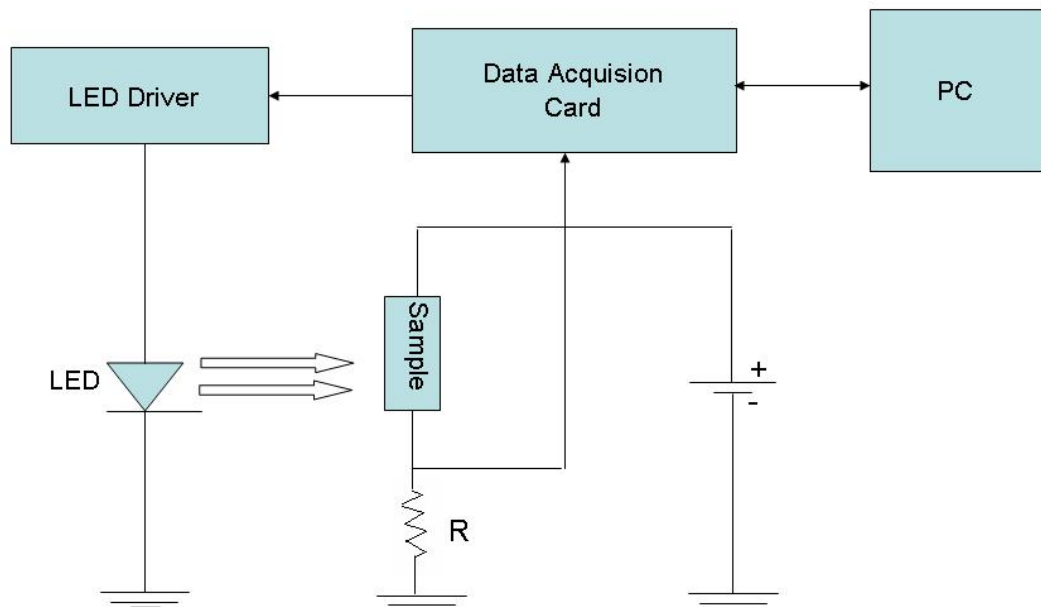
Figure 3.5. The diagram of the photoconductivity experimental set up.

CHAPTER 4

RESULTS AND DISCUSSION

4.1 Introduction

In this chapter, the results of the EDSA, x-ray, reflection and transmission experiments will be analyzed to reveal the structural and optical properties of the $TlInS_2$ crystal. Besides, the results and analysis of the thermally stimulated current experiments will be given to express the defect centers in the crystal and their properties.

4.2 Results of Energy Dispersive Spectral Analysis and X-ray Experiments

The chemical composition of $TlInS_2$ crystal was determined by means of energy dispersive spectroscopic analysis, shown in figure 4.1. The atomic composition ratio of the studied samples (Tl : In : S) was found to be 25.6 : 25.2 : 49.2, respectively.
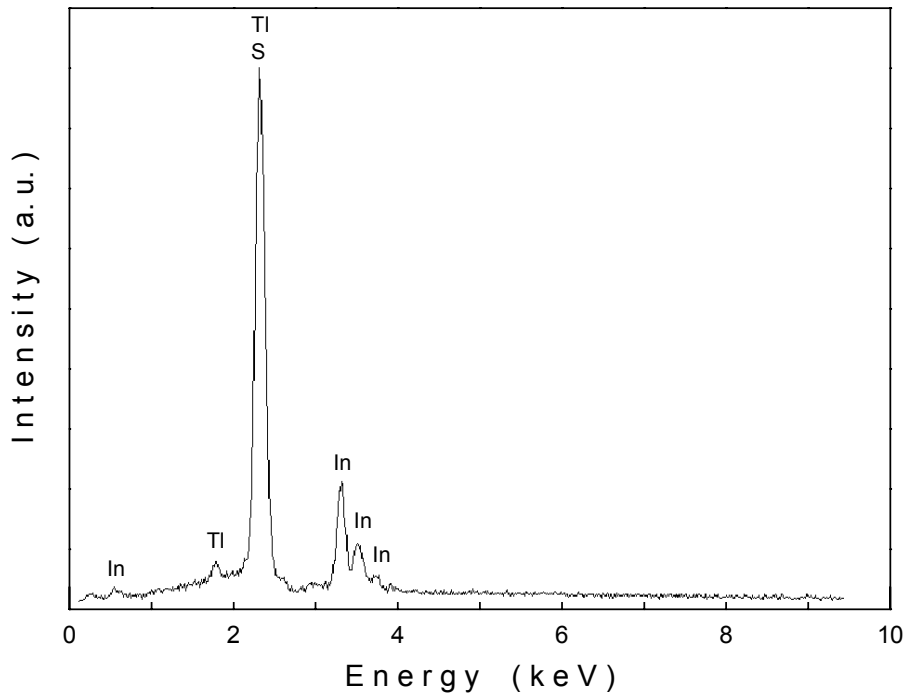
Figure 4.1. Energy dispersive spectroscopic analysis of the TlInS$_2$ crystal.

The structure of TlInS$_2$ crystal was defined by the x-ray powder diffraction experiments. Figure 4.2 shows the x-ray diffractogram of TlInS$_2$ crystal. The crystal system, Miller indices of the diffraction peaks and the lattice parameters were evaluated by using a least-squares computer program "DICVOL 04". Miller indices ($h\ k\ l$) , the observed and calculated interplanar spacings (d) and the relative intensities ($I\ /\ I_0$) of the diffraction lines are given in table 4.1.
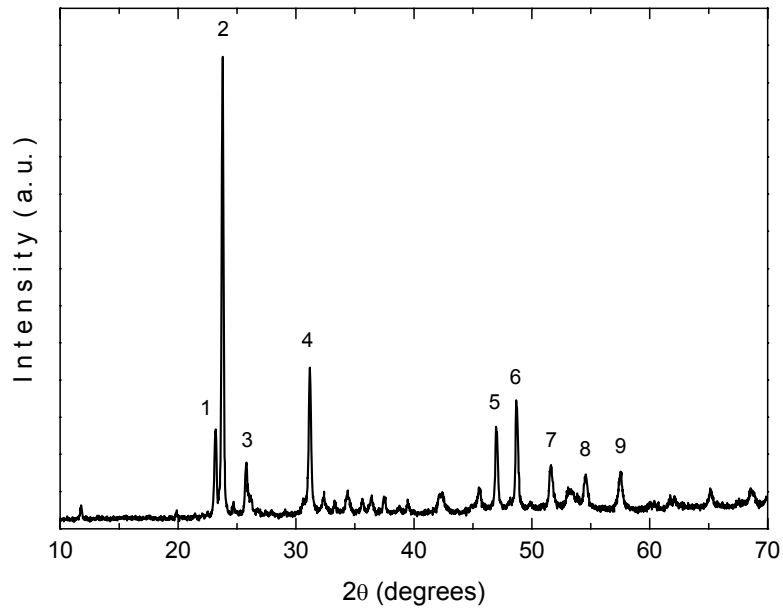
Figure 4.2. X-ray powder diffraction pattern of TlInS$_2$ crystal.

Table 4.1. X-ray powder diffraction data for TlInS$_2$ crystals.

No.	$h\ k\ l$	d_{obs} (nm)	d_{calc} (nm)	I/I_0
1	2 0 0	0.38309	0.38351	21
2	1 0 -1	0.37387	0.37354	100
3	1 1 0	0.34504	0.34529	14
4	3 0 -1	0.28662	0.28635	34
5	0 2 0	0.19333	0.19328	22
6	3 0 -2	0.18690	0.18693	27
7	4 0 2	0.17692	0.17692	14
8	2 1 -2	0.16800	0.16809	12
9	0 0 2	0.16005	0.16000	12

4.3 Results of Reflection and Transmission Experiments

Figure 4.3 presents the transmittance (T) and the reflectivity (R) spectra of TlInS$_2$ crystals registered in the wavelength (λ) range from 400 to 1100 nm. The absorption coefficient α and the refractive index n were calculated using the following relations [35]

$$\alpha = \frac{1}{d} \ln \left\{ \frac{(1-R)^2}{2T} + \left[\frac{(1-R)^4}{4T^2} + R^2 \right]^{1/2} \right\} , \tag{4.1}$$

$$n = \frac{1+R}{1-R} + \left[\frac{4R}{(1-R^2)} - \left(\frac{\alpha\lambda}{4\pi} \right)^2 \right]^{1/2} , \tag{4.2}$$

where d is the sample thickness.

Reflection measurements were carried out using the specimens with natural cleavage planes and the thickness such that $\alpha d \gg 1$. The sample thickness was then reduced (by repeated cleaving using the transparent adhesive tape) until it was convenient for measuring the transmission spectra. The thickness of the sample was determined through the transmission interference fringes at the wavelengths slightly longer than the intrinsic absorption edge, where the sample has relatively high transmission values (figure 4.3). The long wavelength values of the refractive index $n = 2.57$, found from the reflection measurements, was used to determine the thickness of the sample, which turned out to be about 10 μm for room temperature transmission measurements in most of the cases.
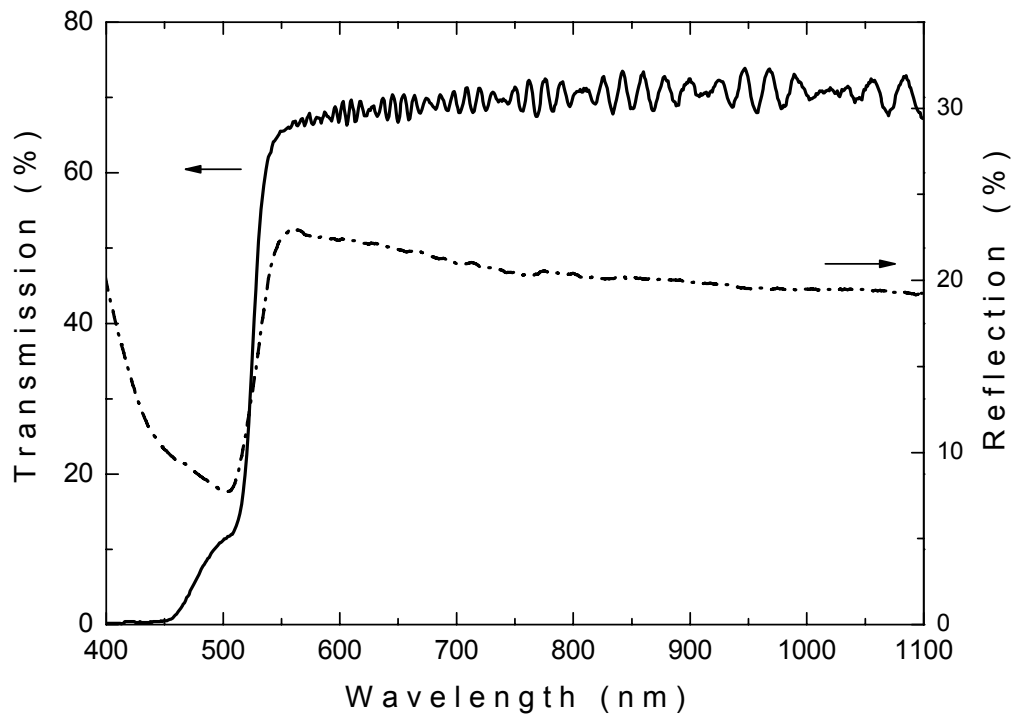
Figure 4.3. The spectral dependencies of transmittance and reflectivity for TlInS$_2$ crystal at $T = 300$ K.

From the analysis of the experimental data, it was revealed that the absorption coefficient α is proportional to $(h\nu - E_g)^p$ with $p = 2$ in the energy range 2.27 - 2.42 eV and $p = 1/2$ in the energy range 2.50 - 2.75 eV. The dependencies of $(\alpha h\nu)^{1/2}$ and $(\alpha h\nu)^2$ on the photon energy $h\nu$ are presented in figure 4.4. Experimental data (circles) were fitted to a linear equation (the solid lines) to find the energy band gaps. The linear dependencies were observed for the relations $(\alpha h\nu)^{1/2}$ and $(\alpha h\nu)^2$ versus $h\nu$. This imply the existence of the indirect and the direct allowed transitions for the TlInS$_2$ crystals over the ranges 2.27 - 2.42 eV and 2.50 - 2.75 eV, respectively. Using the extrapolations of the straight lines down to $(\alpha h\nu)^{1/2} = 0$ and $(\alpha h\nu)^2 = 0$, the values of the indirect and the

44

direct band gap energies were determined as $E_{gi} = 2.27 \pm 0.02$ eV and $E_{gd} = 2.47 \pm 0.02$ eV.
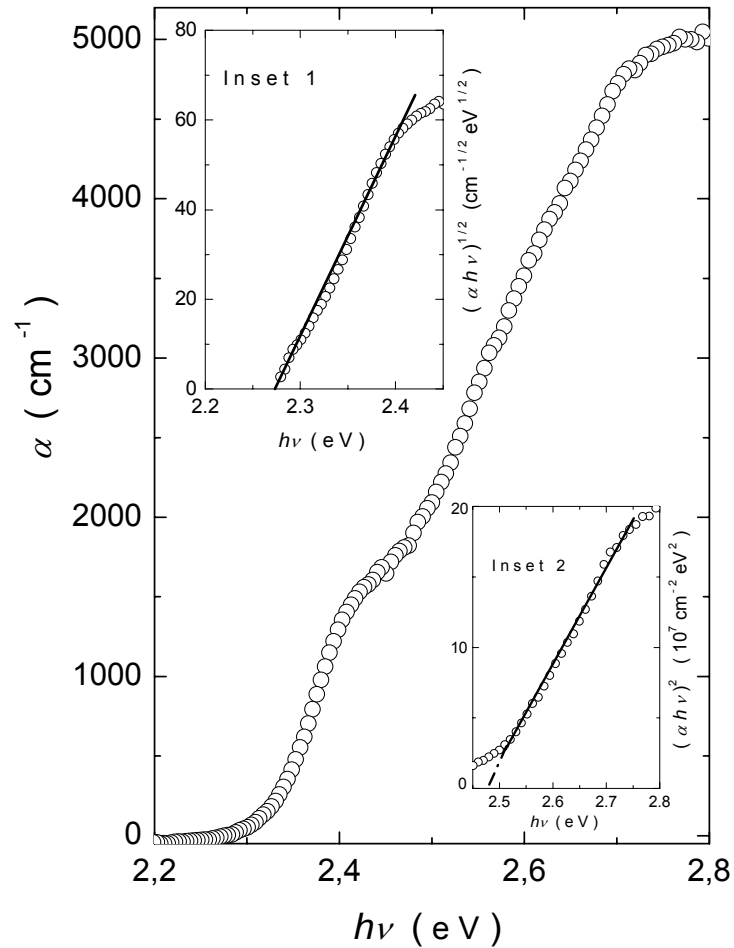
Figure 4.4. The variation of absorption coefficient as a function of photon energy at $T = 300$ K. Insets 1 and 2 represent the dependences of $(\alpha h \nu)^{1/2}$ and $(\alpha h \nu)^2$ on photon energy, respectively.

Figures 4.5 shows the transmission spectra of the TlInS$_2$ crystals that were registered in the temperature range of 10–300 K. The thick samples having the thickness about 300 μm were used in the low temperatures as the thin

layered samples broke into the pieces at low temperatures due to their high fragility. Therefore, we were only able to analyze the temperature dependence of the indirect band gap energy (E_{gi}). Technical reasons did not allow us a direct measurement of the reflectivity spectra at low temperatures. Therefore, for the calculation of absorption coefficient α at low temperatures, the spectral dependence of room temperature reflectivity was uniformly shifted in the energy according to the blue shift of the absorption edge.
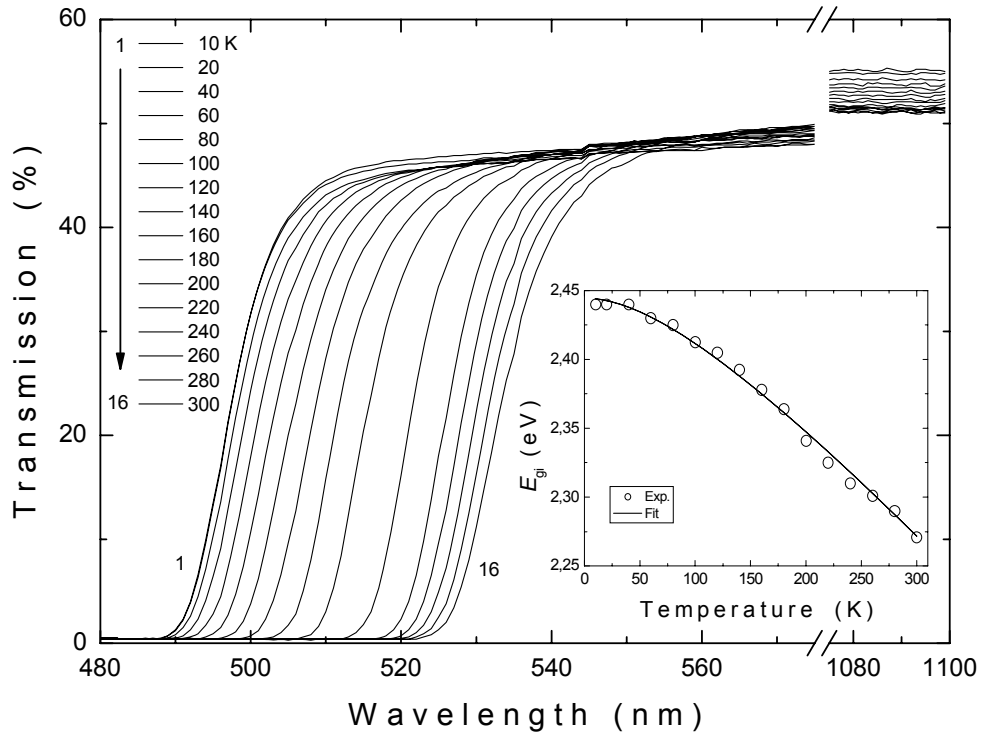
Figure 4.5. The spectral dependences of transmittance for TlInS$_2$ crystal in the temperature range of 10-300 K. Inset: the indirect band gap energy as a function of temperature. The solid line represents the fit using equation 4.3.

The obtained values of the indirect energy gaps decrease in the range 2.44-2.27 eV with the variation temperature from 10 to 300 K, as displayed in

the insets of figure 4.5. The temperature dependence of the energy band gap can be represented by the relation [35]

$$E_{gi}(T) = E_{gi}(0) + \frac{\gamma T^2}{T + \beta} \quad , \tag{4.3}$$

where $E_{gi}(0)$ is the absolute zero value of the band gap, $\gamma = dE_{gi}/dT$ is the rate of change of the band gap with temperature, and β is approximately the Debye temperature. The experimental data for the dependencies of E_{gi} on the temperature (10-300 K) were fitted using equation 4.3 as shown in the inset of figure 4.5 (the solid line correspond to the theoretical fit). The fitting parameters were found to be $E_{gi}(0) = 2.44$ eV, $\gamma = -9.2 \times 10^{-4}$ eV/K, and $\beta = 160$ K for TlInS$_2$ crystals.

Figure 4.6 displays the dependence of the refractive index n on the wavelength that was determined employing equations 4.1 and 4.2. It is possible to observe that the refractive index in the energy region of $hv < E_g$ gradually decreases from 2.85 to 2.57 with increasing wavelength up to 1100 nm. The dispersive refractive index data in $hv < E_g$ range were analyzed according to the single-effective-oscillator model proposed by Wemple and DiDomenico [37, 46]. The refractive index is related to the photon energy through the relationship

$$n^2 = 1 + \frac{E_{so}E_d}{E_{so}^2 - (hv)^2} \quad , \tag{4.4}$$

where E_{so} is the single oscillator energy and E_d is the dispersion energy. Plotting $(n^2 - 1)^{-1}$ versus $(hv)^2$ allows the determination of the oscillator parameters by fitting a linear function to the lower energy data range. The fits of the above reported function is presented in the inset of figure 4.6. The zero-frequency

refractive index n_0 is estimated from equation 4.4, i.e. according to the

expression $n_0^2 = 1 + \dfrac{E_d}{E_{so}}$,
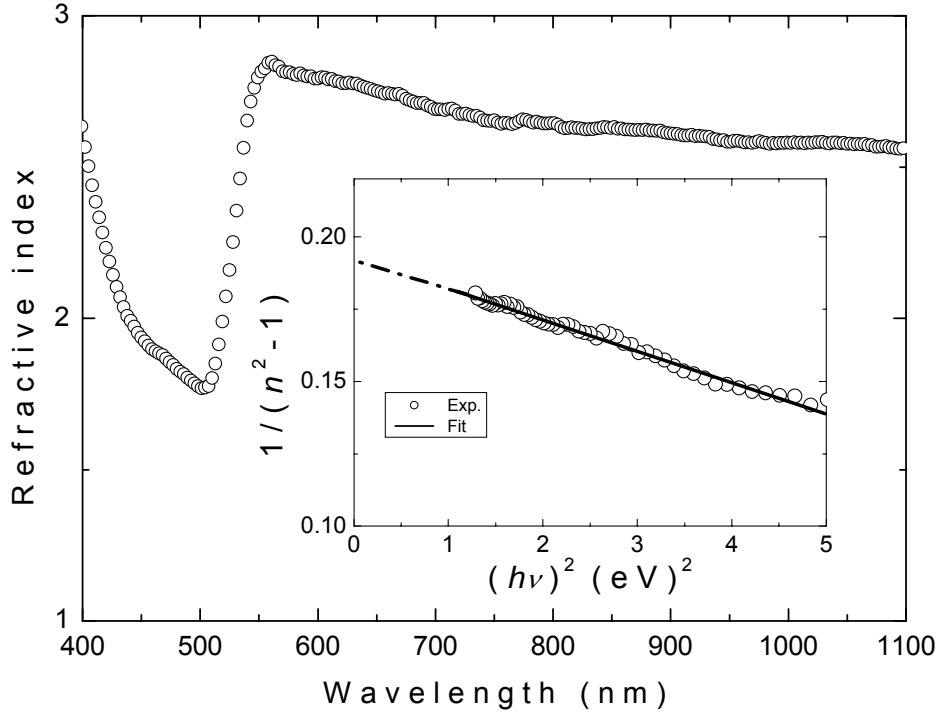
Figure 4.6. The dependence of refractive index on the wavelength for TlInS$_2$ crystal. Inset: Plot of $(n^2-1)^{-1}$ versus $(h\nu)^2$. The solid line represents the fit using equation (4.4).

The values of the parameters E_{so} and E_d were calculated from the slope and the intersection with y-axis of the straight line (inset of figure 4.6) as 4.66 and 24.28 eV. Furthermore, the values of the zero-frequency dielectric constant $\varepsilon_0 = n_0^2 = 6.20$ and the refractive index $n_0 = 2.49$ were evaluated by means of equation 4.4 for TlInS$_2$ crystals. The oscillator energy E_{so} is an "average" energy gap and, to a fair approximation, it is associated empirically with the lowest

direct band gap E_{gd} by the relation $E_{so} \approx 2.0\ E_{gd}$ [38]. The ratio E_{so}/E_{gd}, determined in this study, was found to be 1.87.

At this point, it is worthwhile to compare the dispersive refractive index presented above with those previously reported for the TlInS$_2$ crystals [11, 47-49]. In this study, the determined value of the refractive index, corresponding to the $\lambda = 700$ nm (which was the only common wavelength chosen for the comparison with the results of the other studies), was found to be 2.70. The values of the refractive indices obtained in literature for the same wavelength were equal to 2.54 [50] and 2.68 [11].

4.4. Results of Thermally Stimulated Current Experiments

Thermally stimulated current measurements on TlInS$_2$ crystal were carried out utilizing different experimental conditions (illumination time and temperature, heating rates, etc...) in the low and high temperature ranges. Therefore, TSC results have been reported in two different sections each for low and high temperature ranges, respectively.

4.4.1 Results of TSC Experiments of TlInS$_2$ in the Low Temperature Range 10-100 K

4.4.1.1 Determination of the Type of the Charge Carriers

Figure 4.7 shows a typical TSC curve of TlInS$_2$ crystal measured with heating rate of $\beta = 1.0$ K/s both for forward and reverse bias conditions in the 10-100 K temperature range. When the sample is illuminated in proximity to a contact, both types of carriers are created near the contact. Then depending on the bias voltage, only one type of carrier will be swept through the entire field region, whereas the second type is collected very quickly. Therefore only the former can be trapped. By illumination of the positive and negative contacts of

the sample separately, the maximum TSC measured for the first peak equals 6.0 and 15.3 μA and for the second peak equals 6.4 and 16.4 μA, respectively. The intensity of the current peak was highest when the polarity of the illuminated contact was positive. Therefore the trapping centers corresponding to these peaks can be characterized as hole traps.
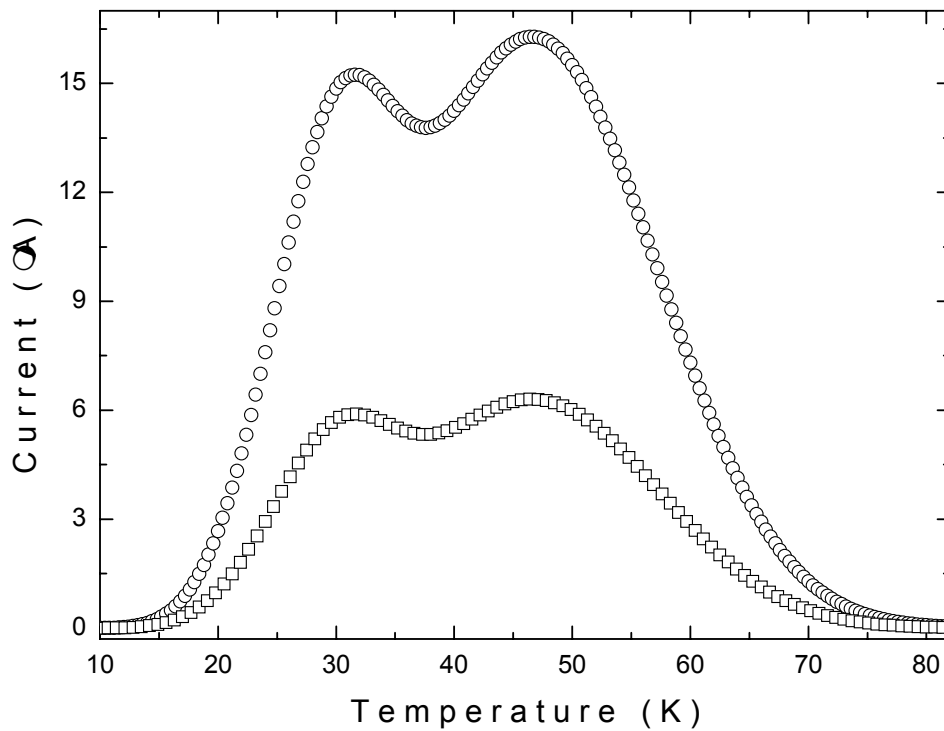
Figure 4.7. Typical experimental TSC curves of TlInS$_2$ crystal under opposite bias voltage. Circles and squares represent the experimental data obtained at illumination of positive and negative contacts, respectively.

4.4.1.2 Determination of Activation Energy

For the analysis of the TSC spectra, it is important to reveal the type of trapping kinetics [51]. The comparison of the relative magnitudes of capture cross sections S_t and S_r of the trapping and recombination centers determines the type of the trapping kinetics. For monomolecular process $S_t << S_r$, the slow retrapping occurs. In the case of slow retrapping, electrons thermally excited from traps are assumed to have much greater probability of recombining with holes than of being retrapped. In this case, the concentration of filled traps has no effect either on the shape of the TSC curve or on the position of the peak. For the case $S_t >> S_r$, fast retrapping occurs. For fast retrapping process, electrons are retrapped large number of times before recombination occurs. Thus, the peak position and shape of the TSC curve depend on the concentration of filled traps. To change the initial density of traps, the TSC spectra of TlInS$_2$ crystal were recorded for different illumination time (0-1000 sec) at constant heating rate of β = 1.0 K/s (figure 4.8). The shape of the TSC spectra and T_{max} values remain almost invariable for different values of illumination time. This result indicates that all the observed traps may be considered under the monomolecular (slow retrapping) conditions. Inset of the figure 4.8 shows the dependence of peak maximum currents on illumination period for each peak. It is possible to observe that traps are filled completely after nearly 900 sec. Therefore, the illumination time for TSC experiments was taken as 900 sec.

51
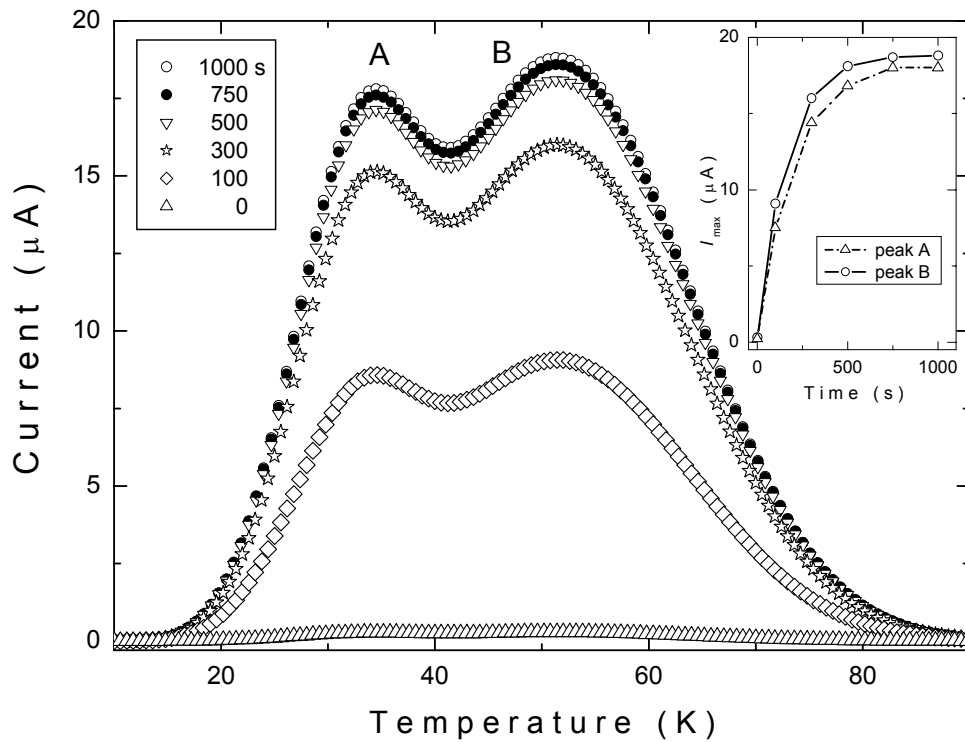
Figure 4.8. TSC spectra of TlInS$_2$ crystal for various illumination times. Heating rate $\beta = 1$ K/s. Inset: the dependence of peak maximum current on illumination time. The dash-dotted lines are only guides for the eye.

Figure 4.9 shows typical TSC spectra of TlInS$_2$ single crystal measured at six linear heating rates of $\beta = 0.3$–1.5 K/s in the 10–100 K temperature range. The thermally stimulated current gradually increases and the temperature for its maximum value (T_{max}) shifts to higher temperature with increasing the heating rate, as expected.
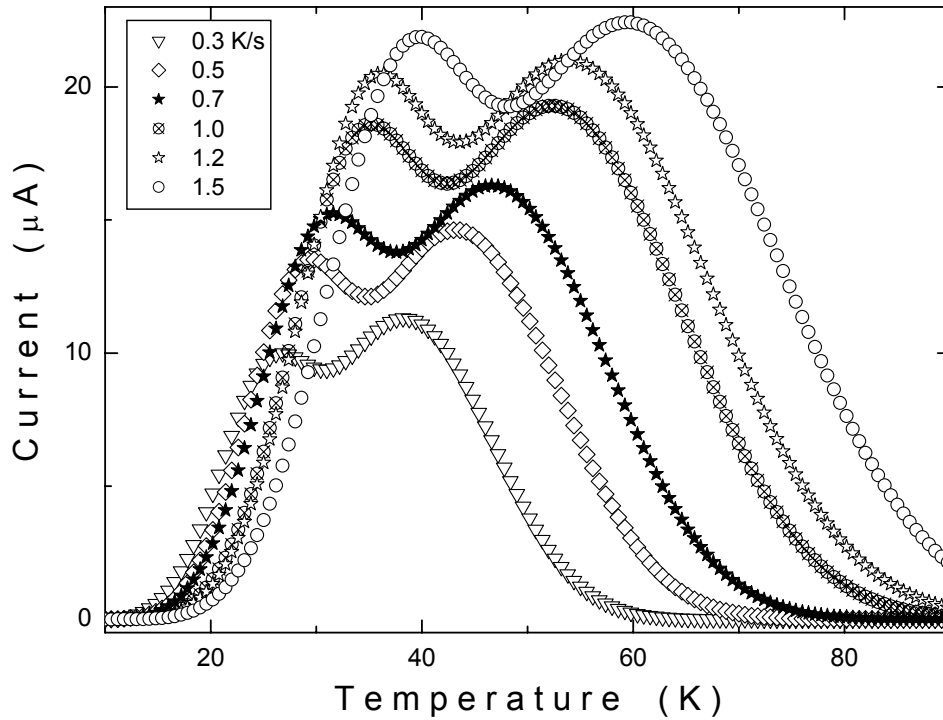
Figure 4.9. Experimental TSC spectra of TlInS$_2$ crystal obtained with various heating rates.

There are several methods to evaluate the trapping parameters from the experimental TSC spectra. The applicability of some methods is restricted if the spectra consist of a number of overlapped peaks. We have used the curve fitting, initial rise, peak shape and isothermal decay methods for the analysis of the present TSC data.

The curve fitting method was used for decomposition of the TSC spectra into separate peaks associated with the charged traps in TlInS$_2$ crystal. When the curve is fitted by means of two peaks (designated A and B), we obtained a good fit to the experimental data. Good agreement has been obtained between the experimental TSC data and fitted curve, computed with the assumption of slow retrapping (figure 4.10). This suggests that retrapping is negligible for the traps

53

of TlInS$_2$ studied in the present work. The solid line in figure 4.10 shows the data for a heating rate of 1.0 K/s fitted with two peaks (A and B) having activation energies of E_{tA} = 12 meV and E_{tB} = 14 meV, respectively (table 4.2).

Table 4.2. The activation energy (E_t), capture cross section (S_t), attempt-to-escape frequency (ν) and concentration (N_t) of traps for two TSC peaks of TlInS$_2$ crystal.

Peak	T_m(K)	E_t (meV)			S_t (cm^2)	ν (s^{-1})	N_t (cm^{-3})
		Curve fitting method	Initial rise method	Peak shape method			
A	32.1	12	12	15	2.2 x 10^{-23}	10.3	2.2 x 10^{13}
B	51.5	14	14	17	7.1 x 10^{-25}	0.9	8.1 x 10^{13}
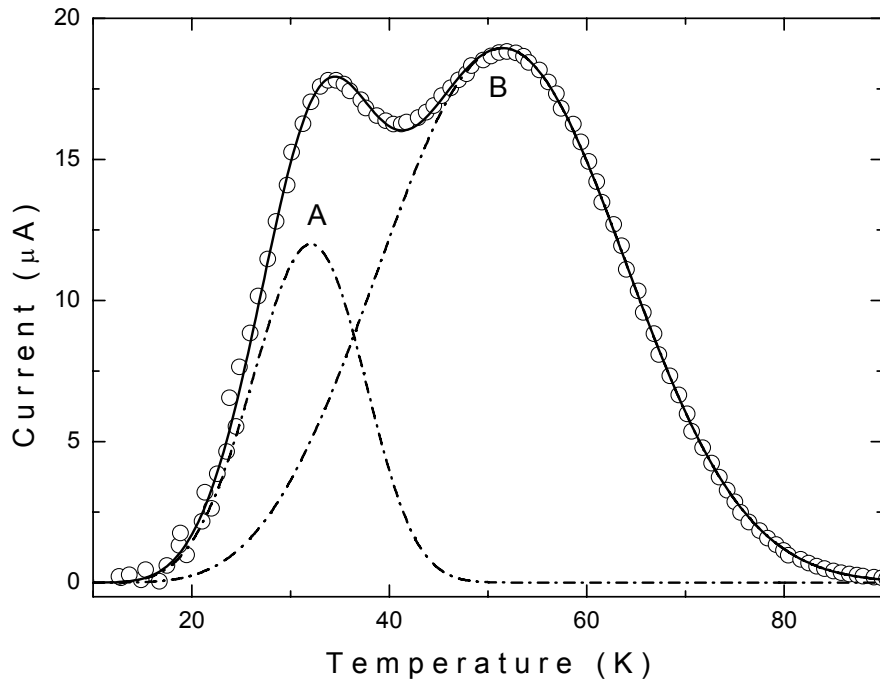
Figure 4.10. Experimental TSC spectrum of TlInS$_2$ crystal with heating rate 1.0 K/s and decomposition of this spectrum into two separate peaks. Open circles are experimental data. Dash-dotted curves represent decomposed peaks. Solid curve shows total fit to the experimental data.

The overlapping TSC peaks were also isolated by applying the "thermal cleaning" procedure [24]. "Thermal cleaning" procedure was applied as follows: The sample was cooled and irradiated at 10 K. Then it was taken through the same heating cycle as before but was stopped at a temperature near T_{mA} which is equal to T_{stop} = 34 K. This way, traps responsible for the current peak for $T <$ T_{mB} were substantially emptied. Then, the crystal was recooled and reheated in the dark at the same rate. This allowed the observation of a sharper TSC peak at a slightly higher temperature due to electrons released from traps which are associated with the TSC maximum centered near T_{mB} (figure 4.11).
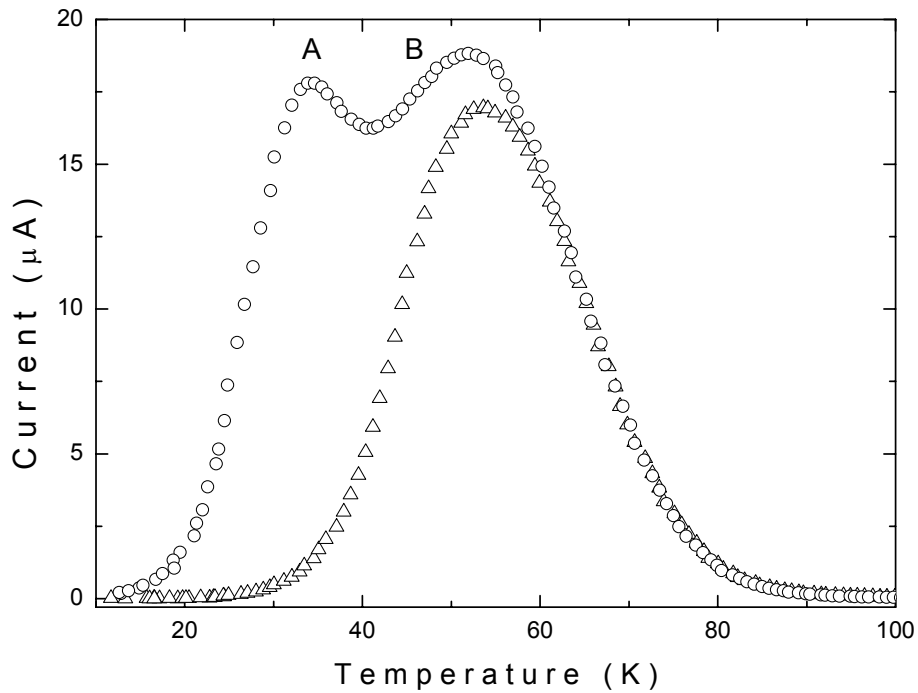
Figure 4.11. Experimental TSC spectra of TlInS$_2$ crystal before (circles) and after (triangles) thermal cleaning. Heating rate $\beta = 1.0$ K/s.

Experimental TSC curves have also been analyzed by using initial rise and peak shape methods. The initial rise method, which is valid for all types of recombination kinetics, is based on the assumption that the TSC is proportional to $\exp\left(-E_t/kT\right)$ when the traps begin to empty with temperature [24]. Thus, a semi-logarithmic plot of the current versus $1/T$ gives a straight line with a slope of $\left(-E_t/k\right)$. The plots for TSC peaks of TlInS$_2$ crystal are shown in figure 4.12.
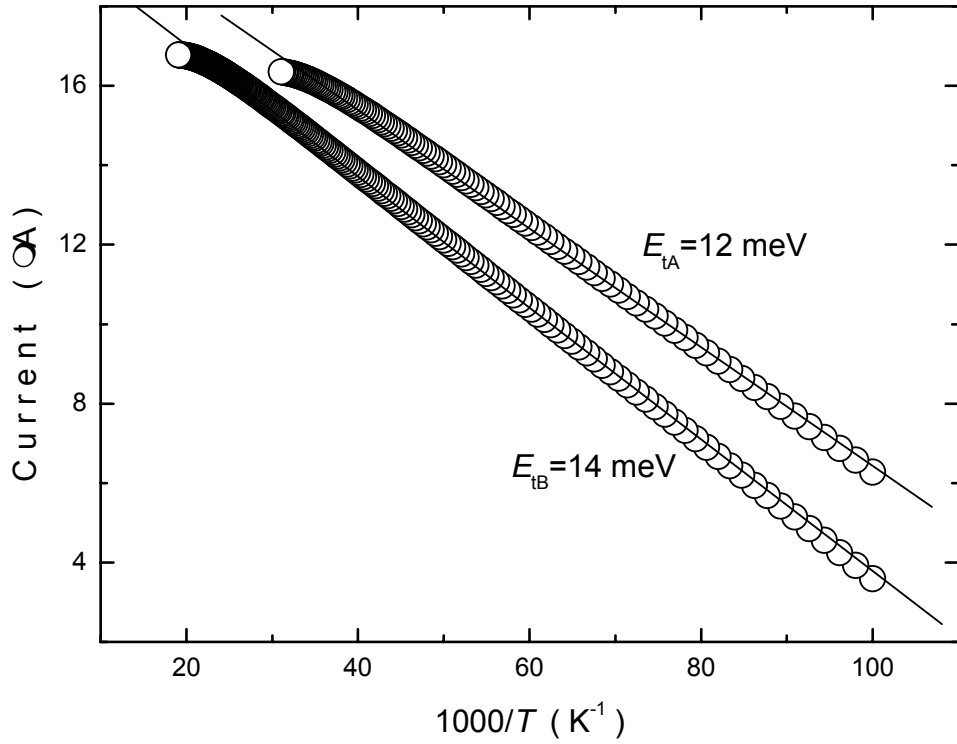
Figure 4.12 Thermally stimulated current vs.1000/T for A- and B-peaks in the TSC spectrum of TlInS$_2$ crystal: the circles show the experimental data and the lines represent the theoretical fits using initial rise method.

The activation energies of traps are also calculated using the peak shape method discussed in section 2.7.5. The averaged values of obtained activation energies E_τ, E_δ and E_w for the peaks are presented in table 4.2.

We also used the isothermal decay method to find the activation energies of the traps. In this method, the sample is heated at a constant rate from an initial temperature to a specific temperature T_p and held at this temperature until complete detrapping. For this process the thermally stimulated current is described by the equation 2.53. The TSC isothermal decay measurements on the TlInS$_2$ crystal were repeated at temperatures T_p = 33, 36, 39, 42 and

45 K (figure 4.13). For these illumination temperatures, the first peak is thermally cleaned from the whole TSC curve and the obtained glow curve is related to the second peak. Then by using the decaying part of the curve, ln (I) versus time graphs were plotted for each data from which the slopes of the straight lines give ($-\gamma$) represented in the equation 2.54. The values of the slopes versus $1/T_p$ give a straight line, from which E_t was obtained as 17 meV (inset of the figure 4.13). The linear intersection of the ln (γ) versus $1/T_p$ graph gives the attempt to escape frequency as $\nu = 3.4$ s^{-1}.
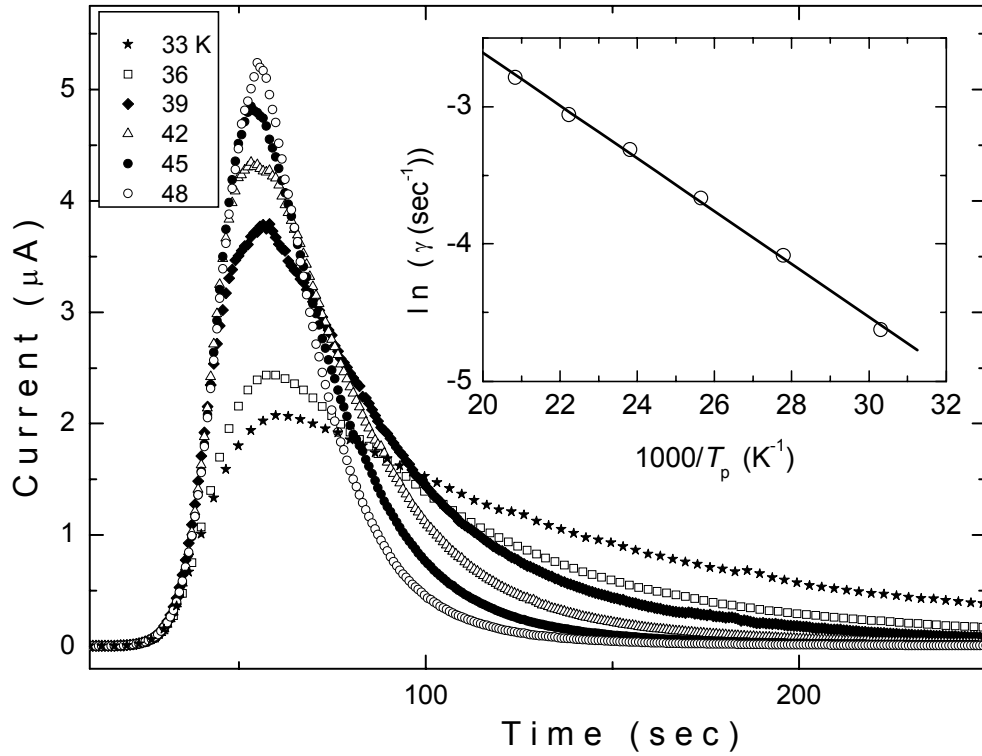
Figure 4.13. Experimental TSC spectra of TlInS$_2$ crystal at different temperatures T_p. Inset: $\gamma = \nu \exp(-E_t / kT_p)$ plot as a function of $1/T_p$.

4.4.1.3 Determination of the Traps Distribution

The analysis of TSC data gives information about the characteristic features of traps distribution. For this regard, the sample was excited by light at different excitation temperatures (T_0) ranging from 18 to 32 K, so as to allow trapping of the photo-produced electrons. Then, the light source was switched off, the sample was kept in dark and cooled to 10 K. Thereafter, the sample is successively heated with a heating rate of 1.0 K/s to excite the trapped electrons into the conduction band. Figure 4.14 shows the experimental TSC spectra for TlInS$_2$ crystal at different excitation temperatures (T_0 = 18, 20, 22, 24, 26, 28, 30 and 32 K). The TSC spectra decreased in intensity and shifted towards higher temperatures with increasing the light excitation temperature. This result supports the validity of a quasi-continuous trap distribution [44, 52-54].

The thermally stimulated current at each excitation temperature T_0 can be described by the following expression [44]

$$I = C \nu \exp\left(-E_t / kT\right), \qquad (4.5)$$

where C is a constant. ln (I) versus $1/T$ plots are the straight lines whose slopes give the values of activation energy E_t at each excitation temperature T_0. The activation energies obtained at different excitation temperatures and the maximum temperatures of thermo-current curves were listed in table 4.3. The activation energy ranges from 17 to 36 meV at T_0 = 18 and 28 K, respectively. We note that above T_0 = 28 K, TSC spectra hard to analyze due to their low intensity.

Table 4.3. TSC parameters for TlInS$_2$ crystal at different excitation temperatures.

Curve	1	2	3	4	5	6
Excitation temperature (K)	18.0	20.0	22.0	24.0	26.0	28.0
Maximum temperature (K)	52.6	53.0	55.0	57.6	60.0	63.7
Curve area (a.u.)	4789	4055	3225	2360	1545	882
Activation energy (meV)	17	21	25	29	33	36

By assuming an exponential traps distribution, whose density at energy E_t will be given by $N = A_1 \exp(-\alpha E_t)$, we can write for the traps filled at the excitation temperature T_0 the following expression [44]

$$S_o \,(I_m / I_e) \propto A_1 \exp(-\alpha E_t), \qquad (4.6)$$

where α is the energy parameter which characterizes the distribution; I_m and I_e are the currents flowing in the crystal at the peak temperature in darkness and during light excitation, respectively; S_o is the area of the TSC peak, which is proportional to the total number of carriers released from the traps during the heating process. Inset of figure 4.14 shows the ln $[S_o\,(I_m / I_e)]$ plotted as a function of the energy E_t, determined from the analysis of TSC curves, which were registered at different excitation temperatures. The graph obtained is a straight line with a slope $\alpha = 0.084$ meV^{-1} corresponding to 27 meV/decade, an order of magnitude variation in the trap density for every 27 meV. A continuous distribution of traps can be expected in a defective semiconductor, since any

60

disorder effect causes a broadening of the energy levels [52]. In particular, the exponential distribution of inset of figure 4.14 is consistent with the presence of fluctuations in the crystal potential, caused by structural defects, like stacking faults in the layered structure, which give rise to real localized states in the forbidden energy gap acting as traps for the carriers.
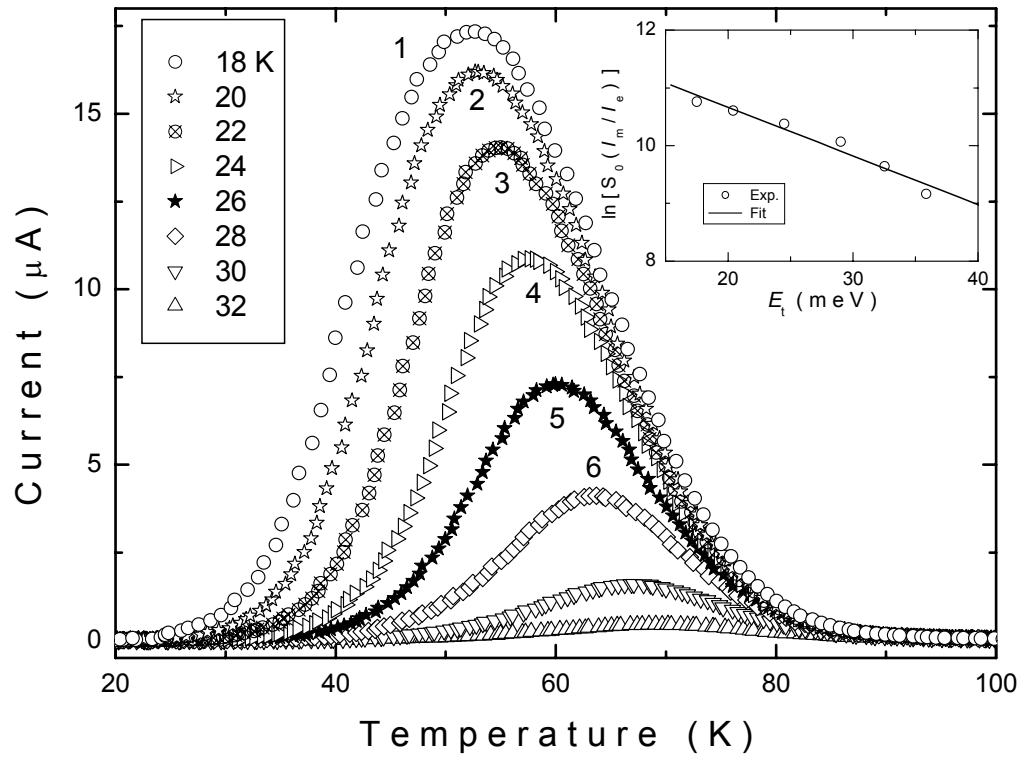

Figure 4.14. Experimental TSC spectra of the TlInS$_2$ crystal at different excitation temperatures T_0. The heating rate was $\beta = 1.0 \, \text{K/s}$. Inset $\ln[S_0(I_m / I_e)]$ plot as a function of the activation energy E_t.

4.4.1.4 Determination of Capture Cross Section and Concentration of the Traps

Once the curve has been fitted and the values of E_t and T_m for peaks are determined (table 4.2), equations 2.40 and 2.35 can be used to calculate B' and the attempt-to-escape frequency ν, respectively. Knowing the value of ν, one can calculate the capture cross section of the traps according to expression 2.46. For the calculation of N_c and υ_{th} we used the electron effective mass $m_e^* = 0.14\ m_o$ reported for TlInS$_2$ crystals [10]. The results obtained for the capture cross section and attempt-to-escape frequency of A- and B-peaks are presented in table 4.2. The small values of the capture cross section justify the assumption of monomolecular kinetics.

The concentration of the traps was estimated using the relation 2.47 and the phoconductivity gain G was calculated from the expression 2.48. The carrier lifetime was determined from the photoconductivity decay experiments [55]. The photo current decay is nearly exponential after termination of light pulse at $t = t_0$. The carrier lifetime τ was determined from the corresponding output voltage expressed as [55]

$$V_{ph} = V_{pho} + D\exp(-t/\tau). \tag{4.7}$$

where V_{pho} is the voltage at $t = \infty$ and D is a constant. Figure 4.15 shows the theoretical fits to the experimental data using equation 4.7 for TlInS$_2$ crystals. The carrier lifetimes were obtained as 21.6 and 20.0 ms for temperatures 33 and 53 K from the decay of the photocurrent. The corresponding photoconductivity gains were found to be 2690 and 2490 from the equation 2.48, using $V = 100$ V and $\mu = 28$ cm^2/Vs [56]. Then the value of N_t obtained for traps is evaluated as $N_{tA} = 2.2 \times 10^{13}$ cm^{-3} and $N_{tB} = 8.1 \times 10^{13}$ cm^{-3} for each peak and presented in the table 4.2.

(a)

(b)
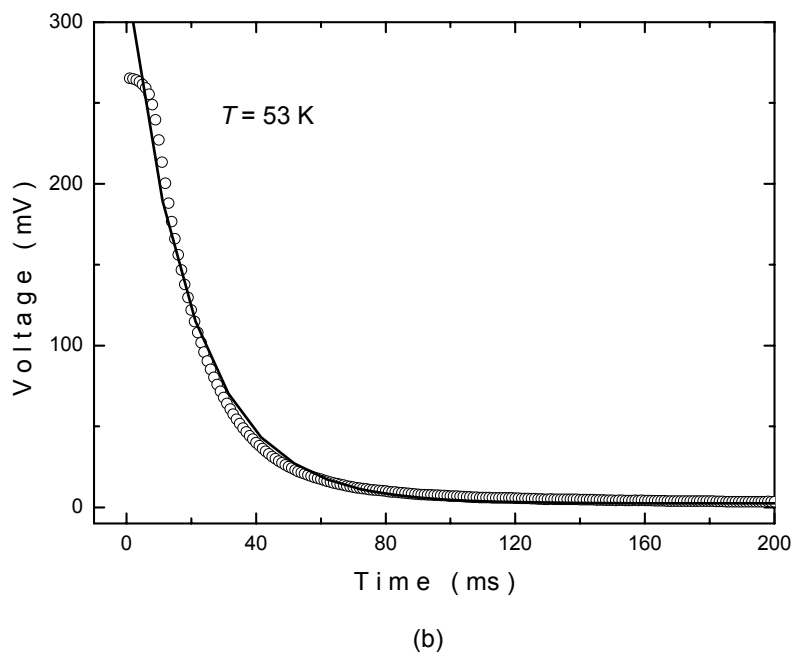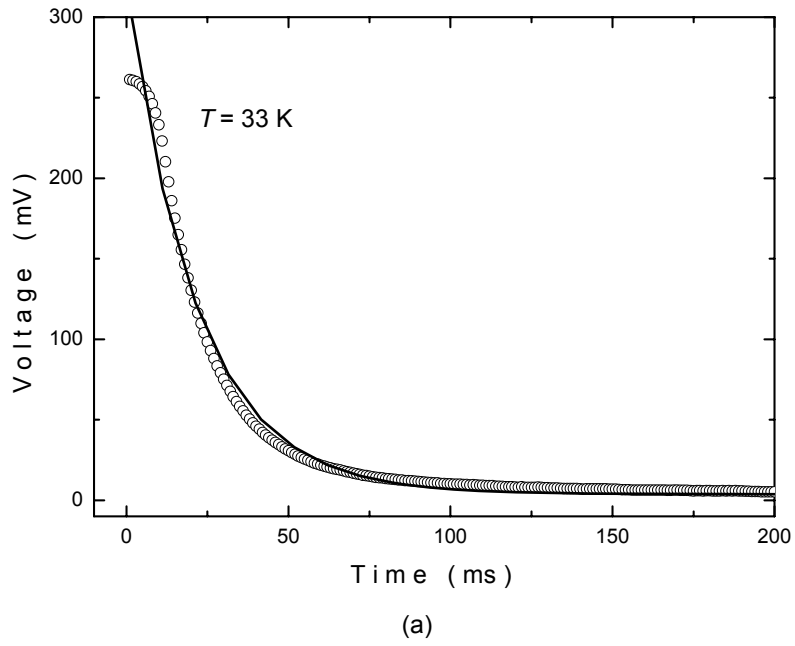
Figure 4.15. Photoconductivity decay curves for the TlInS$_2$ crystal at (a) T = 33 K, (b) T = 53 K.

4.4.2 Results of TSC Experiments of TlInS$_2$ Crystal in the High Temperature Range 100-250 K

4.4.2.1 Determination of the Type of the Charge Carriers

The type of the charge carriers of the high temperature peaks is determined by the method described in section 4.4.1. Figure 4.16 shows a typical TSC curve of TlInS$_2$ crystal measured with heating rate of $\beta = 0.8$ K/s both for forward and reverse bias conditions in the 120-250 K temperature range. By illumination of the positive and negative contacts of the sample separately, the maximum TSC measured for the first peak equals 29 and 98 nA, respectively and for the second peak equals 35 and 86 nA, respectively. The intensity of the current peak was highest when the polarity of the illuminated contact was positive. Therefore the trapping centers corresponding to these peaks can be characterized as hole traps.

Figure 4.16. Typical experimental TSC curves of TlInS$_2$ crystal under opposite bias voltage. Circles and squares represent the experimental data obtained at illumination of positive and negative contacts, respectively.

4.4.2.2 Determination of Activation Energy

The type of the trapping kinetics plays an important role to analyze the TSC spectra. As discussed in the determination of the trapping kinetics for low temperature peaks, in slow and fast retrapping processes TSC curve shows different behaviors with the change of the concentration of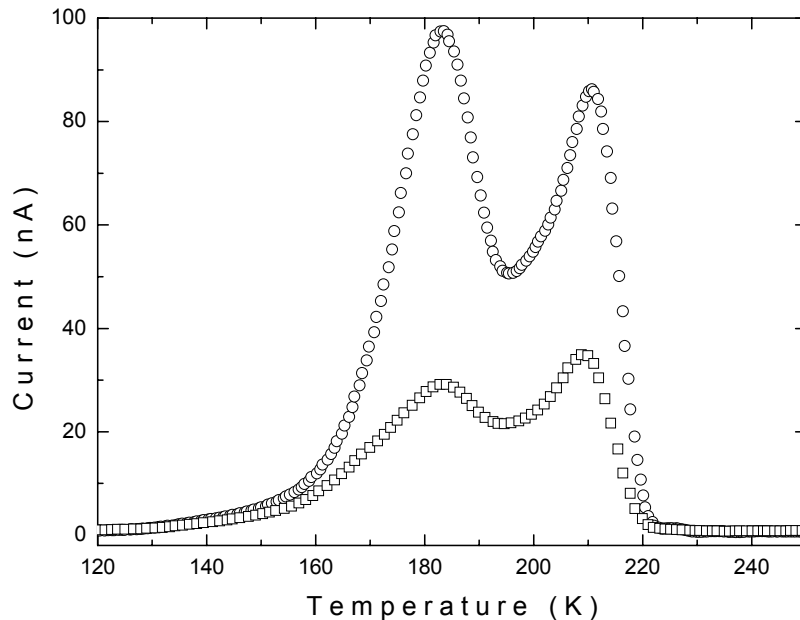 filled traps. In the case of slow retrapping, the concentration of filled traps has no effect either on the shape of the TSC curve or on the position of the peak whereas the peak position and shape of the TSC curve depend on the concentration of filled traps in the case of fast retrapping. To change the concentration of filled traps, the TSC spectra of TlInS$_2$ crystal were recorded for different illumination time (50-1500 sec) at constant heating rate of $\beta = 0.8$ K/s (figure 4.17). The shape of the TSC spectra and T_{max} values remain almost invariable for different values of illumination time. This result indicates that all the observed traps may be considered under the monomolecular (slow retrapping) conditions. Inset of the figure 4.17 shows the dependence of peak maximum currents on illumination period for each peak. It is possible to observe that the traps are filled completely after 1200 sec illumination time. Therefore, TSC measurements were carried out in the high temperature range for 1200 sec illumination time.
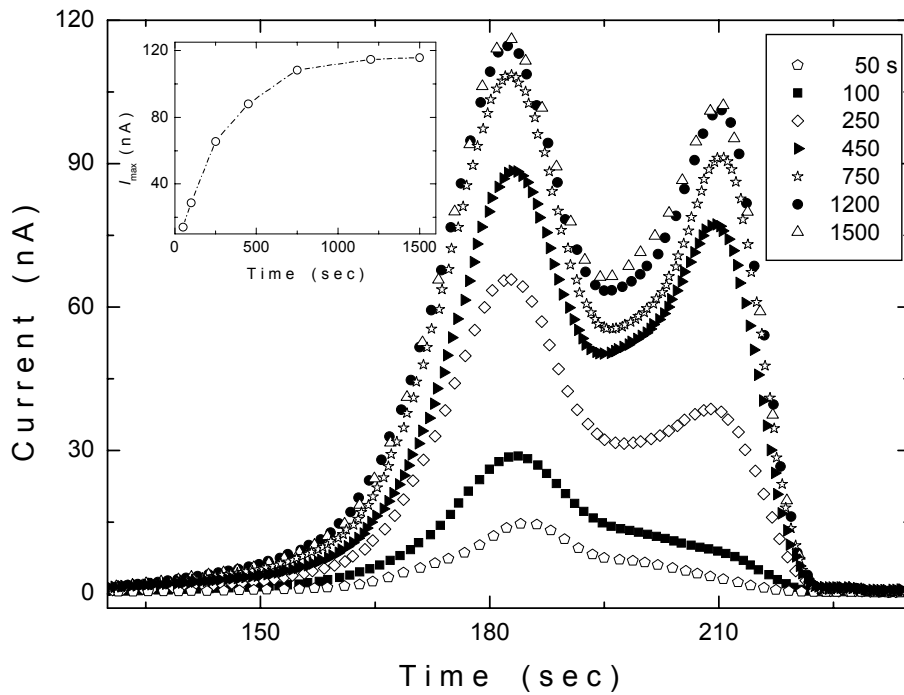
Figure 4.17. TSC spectra of TlInS$_2$ crystal for various illumination times. Heating rate $\beta = 0.8$ K/s. Inset: the dependence of peak maximum current on illumination time for first peak. The dash-dotted line is only guide for the eye.

Figure 4.18 shows typical TSC spectra of TlInS$_2$ single crystal measured at four linear heating rates of $\beta = 0.2$–0.8 K/s in the 120–240 K temperature range. The thermally stimulated current gradually increases and the temperature for its maximum value (T_{max}) shifts to high temperature with increasing the heating rate, as expected.

66
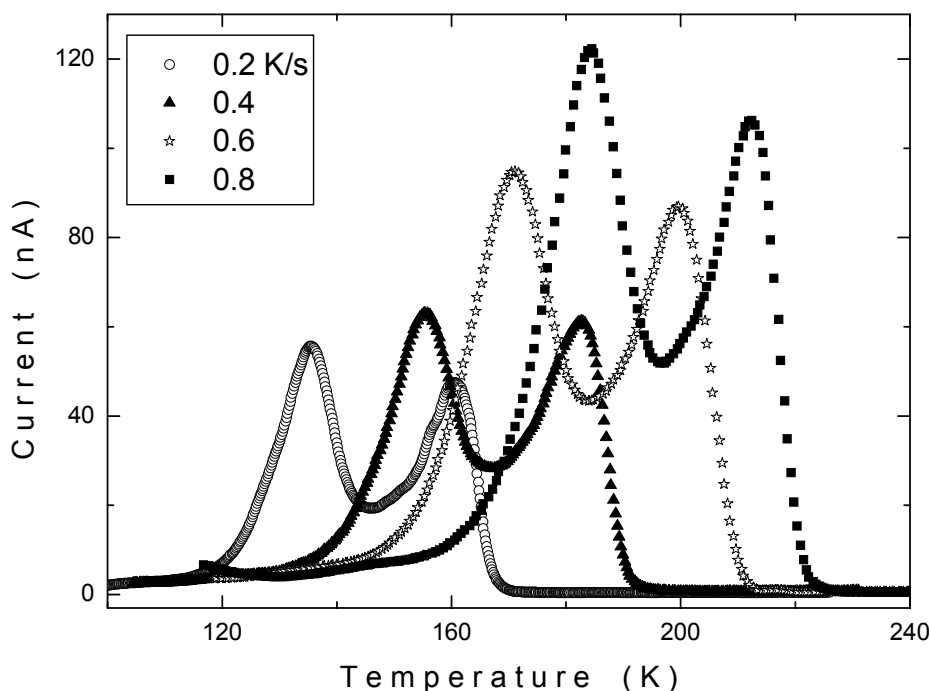
Figure 4.18. Experimental TSC spectra of TlInS$_2$ crystal obtained with various heating rates.

There are several methods to evaluate the trapping parameters from the experimental TSC spectra. The applicability of some methods is restricted if the spectra consist of a number of overlapped peaks. We have used the curve fitting, initial rise and peak shape methods for the analysis of the present TSC data.

The curve fitting method was used for decomposition of the TSC spectra into separate peaks associated with the charged traps in TlInS$_2$ crystal. When the curve is fitted by means of three peaks (designated A, B and C), we obtained a good fit to the experimental data. Good agreement has been obtained between the experimental TSC data and theoretical curve, computed with the assumption of slow retrapping (figure 4.19). This suggests that retrapping is negligible for the traps of TlInS$_2$ studied in the present work. The solid line in

figure 4.19 shows the data for a heating rate of 0.8 K/s fitted with three peaks (A, B and C) having activation energies of E_{tA}= 400 meV, E_{tB} = 570 meV and E_{tC} = 650 meV, respectively (table 4.4).
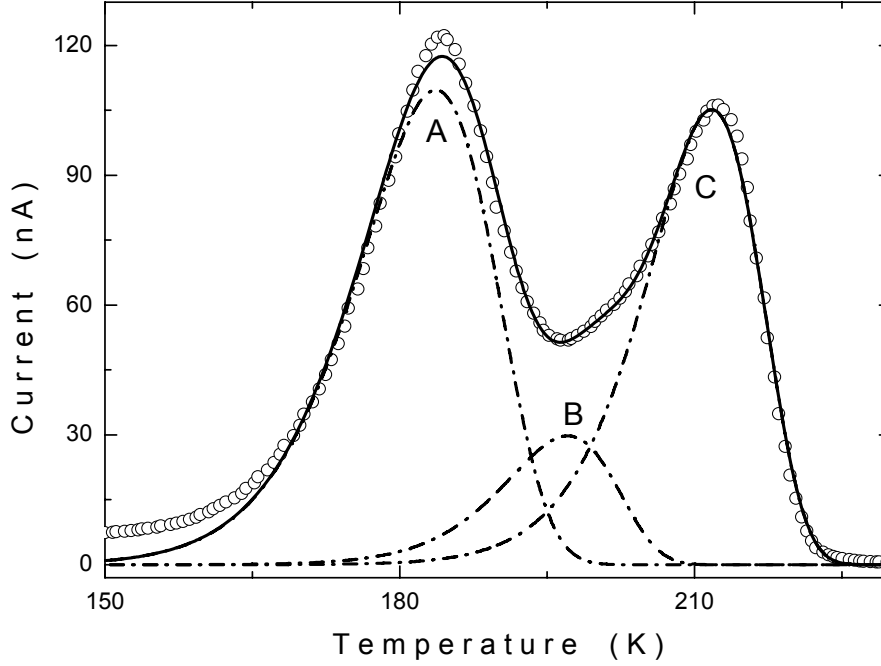
Figure 4.19. Experimental TSC spectrum of TlInS$_2$ crystal with heating rate 0.8 K/s and decomposition of this spectrum into three separate peaks. Open circles are experimental data. Dash-dotted curves represent decomposed peaks. Solid curve shows total fit to the experimental data.

Table 4.4. The activation energy (E_t), capture cross section (S_t), attempt-to-escape frequency (ν) and concentration (N_t) of traps for three TSC peaks of TlInS$_2$ crystal.

Peak	T_m(K)	E_t (meV)			S_t (cm^2)	ν (s^{-1})	N_t (cm^{-3})
		Curve fitting method	Initial rise method	Peak shape method			
A	184	400	400	360	6.3 x10^{-16}	9.6 x 10^9	4.1 x 10^9
B	197	570	570	630	2.7 x 10^{-12}	4.8 x 10^{13}	0.9 x 10^9
C	212	650	650	570	1.8 x 10^{-11}	3.7 x 10^{14}	2.6 x 10^9

The overlapping TSC peaks were also isolated by applying the "thermal cleaning" procedure [24]. "Thermal cleaning" procedure was applied as described in section 4.4.2. The sample was cooled and irradiated at 60 K. Then it was taken through the same heating cycle as before but was stopped at a temperature which is equal to T_{stop} = 150 K. Then, the crystal was recooled and reheated in the dark at the same rate. The resultant thermally stimulated curve after thermal cleaning is shown in figure 4.20. Because the intensity of the B peak is low, it was difficult to observe this peak after thermal cleaning.
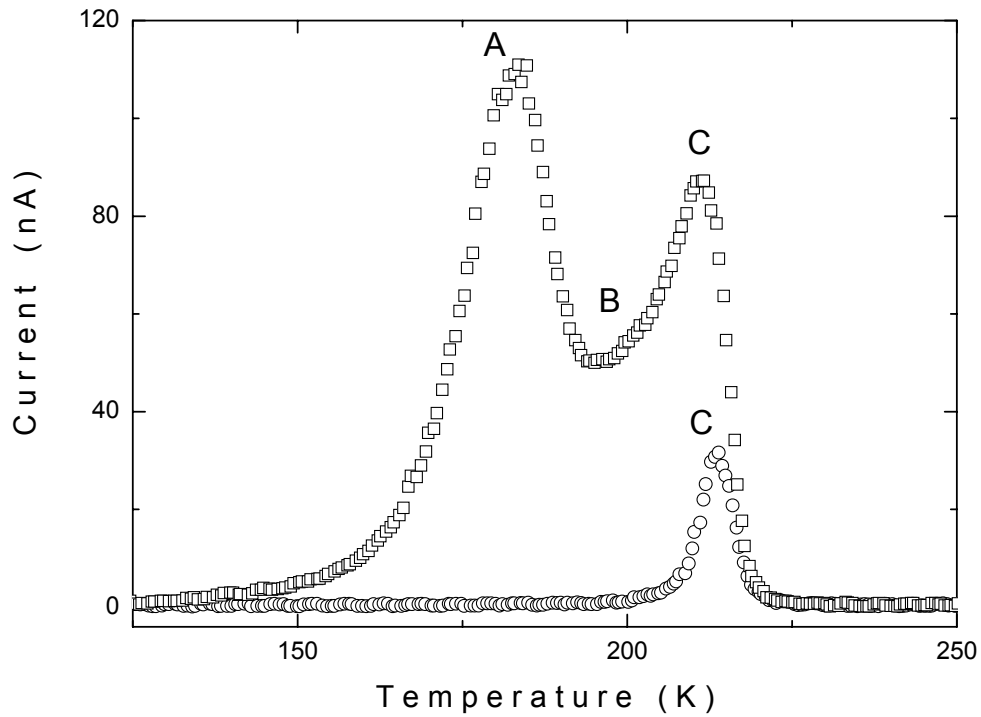
Figure 4.20. Experimental TSC spectra of TlInS$_2$ crystal before (squares) and after (circles) thermal cleaning. Heating rate β = 0.8 K/s.

Experimental TSC curves have also been analyzed by using initial rise and peak shape methods. For the analysis of initial rise method discussed in

69

section 2.7.4, the graphs of the ln (I) versus $1/T$ for TSC peaks of TlInS$_2$ crystal are plotted and shown in the figure 4.21. The activation energies of the traps calculated by this method were found to be 400 meV, 570 meV and 650 meV and presented in table 4.4.
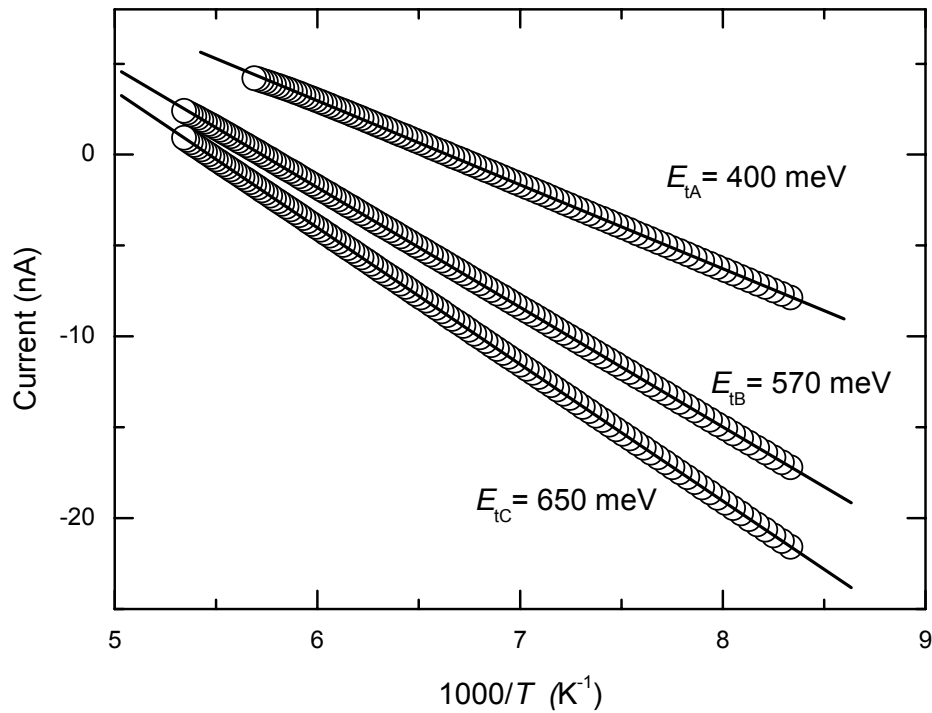
Figure 4.21. Thermally stimulated current vs.1000/T for A-, B- and C-peaks in the TSC spectrum of TlInS$_2$ crystal: the circles show the experimental data and the lines represent the theoretical fits using initial rise method.

The activation energy of traps is also evaluated by using peak shape method. E$_\tau$, E$_\delta$ and E$_w$ can be determined by using equations 2.50, 2.51 and 2.52. The averaged values of obtained activation energies E$_\tau$, E$_\delta$ and E$_w$ for the peaks are reported in table 4.4.

4.4.2.3 Determination of the Traps Distribution

The analysis of TSC data gives information about the characteristic features of traps distribution. For this regard, the sample was excited by light at different excitation temperatures (T_0) ranging from 105 to 120 K, so as to allow trapping of the photo-produced electrons. Then, the light source was switched off, the sample was kept in darkness and cooled to 60 K. Thereafter the sample is successively heated with linear rate of 0.8 K/s to excite the trapped electrons into the conduction band. Figure 4.22 shows the experimental TSC spectra for TlInS$_2$ crystal at different excitation temperatures (T_0 = 105, 110, 115 and 120 K). The TSC spectra decreased in intensity and shifted towards higher temperatures with increasing the light excitation temperature. This fact supports the validity of a quasi-continuous trap distribution [44, 52-54].

The thermally stimulated current at each excitation temperature T_0 can be described by the expression 4.5. The activation energies obtained at different excitation temperatures and the maximum temperatures of thermo-current curves were listed in table 4.5. The activation energy ranges from 730 to 1000 meV at T_0 = 105 and 120 K, respectively.

By assuming an exponential traps distribution the energy parameter α is obtained by drawing the plot of ln [S_o (I_m / I_e)] as a function of energy E_t as mentioned in the calculation of α for low temperature peaks. Inset of figure 4.22 shows the ln [S_o (I_m / I_e)] plotted as a function of the energy E_t determined from the analysis of TSC curves, which were registered at different excitation temperatures. The graph obtained is a straight line with a slope α = 0.0029 meV^{-1} corresponding to 800 meV/decade, an order of magnitude variation in the trap density for every 800 meV.

Table 4.5. TSC parameters for TlInS$_2$ crystal at different excitation temperatures

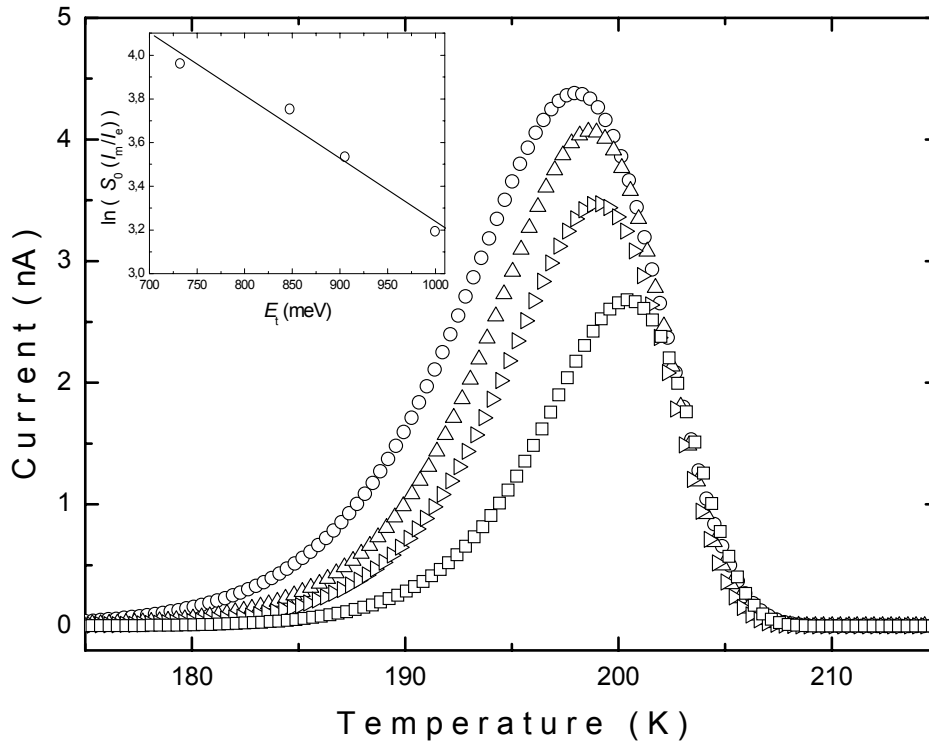| Curve	1	2	3	4
Excitation temperature (K)	105	110	115	120
Maximum temperature (K)	198.0	198.7	199.0	200.0
Curve area (a.u.)	526	427	343	244
Activation energy (meV)	730	850	905	1000

Figure 4.22. Experimental TSC spectra of the TlInS$_2$ crystal at different excitation temperatures T_0. The heating rate was $\beta = 0.8\,\mathrm{K/s}$. Inset: $\ln[S_0(I_m/I_e)]$ plot as a function of the activation energy E_t.

4.4.2.4 Determination of Capture Cross Section and Concentration of the Traps

Once the curve have been fitted and the values of E_t and T_m for peaks are determined (table 4.4), equations 2.40 and 2.35 were used to calculate B and the attempt-to-escape frequency ν, respectively. Knowing the value of ν, one can calculate the capture cross section of the traps according to expression 2.46. For the calculation of N_c and υ_{th} we used the electron effective mass $m_e^* = 0.14$ m_o reported for TlInS$_2$ crystals [10]. The results obtained for the capture cross section and attempt-to-escape frequency of A-, B- and C-peaks are presented in table 4.4. The small values of the capture cross section justify the assumption of monomolecular kinetics. The concentration of the traps was estimated using the relation 2.47. To calculate the photoconductivity gain G, the carrier lifetime is obtained from the photoconductivity decay experiments and analysis as mentioned in section 4.4.1. The photoconductivity decay curve for each peak is shown in figure 4.23. The carrier lifetime was obtained as 17.2, 19.0 and 21.6 ms for temperatures 184, 197 and 212 K, respectively, from the decay of the photocurrent. The corresponding photoconductivity gain was calculated from the expression 2.48 and found to be 2140, 2360 and 2690 using $V = 100$ V and $\mu = 28$ cm^2/Vs [56]. Then the values of N_t obtained for traps are evaluated as 4.1 x 10^9 cm^{-3} , 0.9 x 10^9 cm^{-3} and 2.6 x 10^9 cm^{-3} for peaks A, B and C, respectively, and presented in the table 4.4.
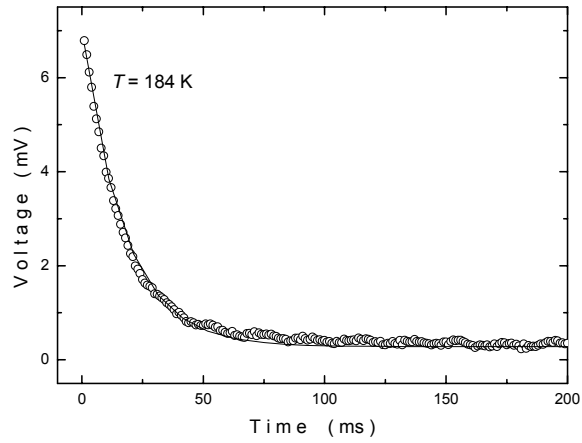
(a)
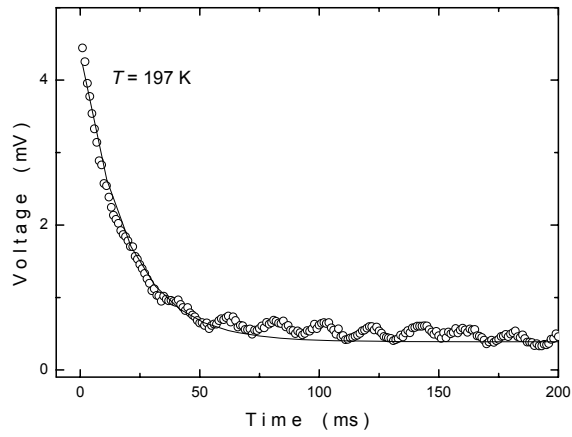
(b)
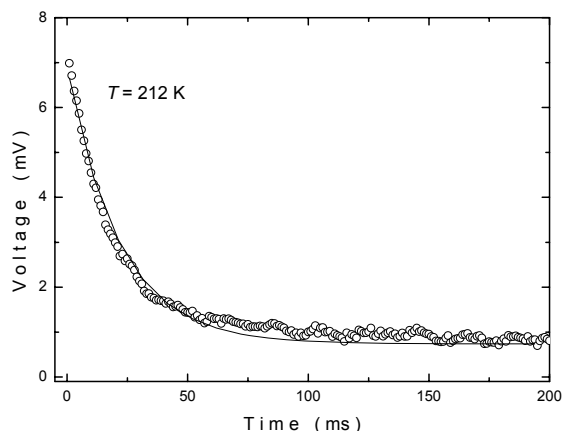
(c)

Figure 4.23. Photoconductivity decay curves for the TlInS$_2$ crystal at (a) T = 184 K, (b) T = 197 K and (c) T = 212 K.

CHAPTER 5

CONCLUSION

In the present thesis, mainly the trap centers and distributions in $TlInS_2$ were studied in the wide temperature range by using thermally stimulated currents technique. In addition, energy dispersive spectral analysis, x-ray and transmission-reflection experiments were employed to determine the atomic composition ratio, lattice parameters and the energy band gaps of as-grown $TlInS_2$ layered single crystals.

The chemical composition of $TlInS_2$ crystals was determined from energy dispersive spectroscopic analysis. The atomic composition ratio of the studied samples (Tl : In : S) was found to be 25.6 : 25.2 : 49.2, respectively. The parameters of monoclinic unit cell were found by studying the x-ray powder diffraction. The Miller indices ($h\ k\ l$), the observed and calculated interplanar spacings (d), and the relative intensities ($I\ /\ I_0$) of the diffraction lines were obtained. The lattice parameters of the monoclinic unit cell were estimated as $a = 0.3763$, $b = 0.3864$, $c = 0.7726$ nm, and $\beta = 97.31°$.

The transmission and reflection spectra of $TlInS_2$ crystals were measured over the spectral region of 400-1100 nm to derive the absorption coefficient and the refractive index. The analysis of the room temperature absorption data revealed the coexistence of the indirect and the direct transitions with the energy band gaps of $E_{gi} = 2.27$ eV and $E_{gd} = 2.47$ eV. The absorption edge was observed to shift toward the lower energy values as temperature increases from 10 to 300 K. These data were used to calculate the indirect energy band gap of the crystal as a function of the temperature. The rate of the change of the

indirect band gap with temperature was obtained as -9.2×10^{-4} eV/K. The absolute zero value of the band gap energy was found to be $E_{gi}(0) = 2.44$ eV. The refractive index dispersion data were analyzed using the single oscillator model. As a result, the oscillator and the dispersion energies, and the zero-frequency refractive index were determined.

Two trapping centers at 12 and 14 meV have been detected in TlInS$_2$ crystals by the TSC technique in the low temperature range 10-100 K. The capture cross sections of the traps were calculated to be 2.2×10^{-23} and 7.1×10^{-25} cm^2. Also the concentrations of the traps were estimated to be 2.2×10^{13} and 8.1×10^{13} cm^{-3}. Thermally stimulated current experiments showed the presence of an exponential distribution of electron-trapping states in TlInS$_2$ crystal. The variation of one order of magnitude in the trap density for every 27 meV was obtained.

Thermally stimulated current experiments in the high temperature range 100-250 K showed that there were three trapping centers at 400, 570 and 650 meV in TlInS$_2$ crystals. Capture cross sections of these traps were calculated to be 6.3×10^{-16}, 2.7×10^{-12} and 1.8×10^{-11} cm^2. Also the concentrations of the traps were estimated to be 4.1×10^9, 0.9×10^9 and 2.6×10^9 cm^{-3}. The experiments on thermally stimulated current show also the presence of an exponential distribution of electron-trapping states in TlInS$_2$ crystal in the high temperature range. The variation of one order of magnitude in the trap density for every 800 meV was obtained.

As the crystals studied are not intentionally doped, the observed levels are thought to originate from defects, created during the growth of crystals and/or unintentional impurities. Various methods are used to calculate the trap parameters and they agree well with each other. The retrapping process is negligible for these levels, as confirmed by the good agreement between the experimental results and the theoretical predictions of the model that assumes slow retrapping.

REFERENCES

[1]   K. A. Yee and A. Albright, *J. Am. Chem. Soc*. **113**, 6474 (1991) and references therein.

[2]   K. R. Allakhverdiev, *Solid State Commun*. **111**, 253 (1999).

[3]   T. D. Ibragimov and I. I. Aslanov, *Solid State Commun*. **123**, 339 (2002).

[4]   H. Hahn and B. Wellmann, *Naturwissenschaften* **54**, 42 (1967).

[5]   D. Muller, F. E. Poltmann, and H. Hahn, *Z. Naturf.* B **29**, 117 (1974).

[6]   K. J. Range, G. Engert, W. Muller, and A. Weiss, *Z. Naturf.* B **29**, 181 (1974).

[7]   N. Kalkan, D. Papadopoulos, A. N. Anagnostopoulos, and J. Spyridelis, *Mat. Res. Bull.* **28**, 693 (1993).

[8]   M. P. Hanias, A. N. Anagnostopoulos, K. Kambas, and J. Spyridelis, *Phys.* (b) **160**, 154 (1989).

[9]   M. P. Hanias, A. N. Anagnostopoulos, K. Kambas, and J. Spyridelis, *Mat. Res.Bull*. **27**, 25 (1992).

[10]   A. F. Qasrawi and N. M. Gasanly, *Cryst. Res. Technol*. **39**, 439 (2004).

[11]   J. A. Kalomiros and A. N. Anagnostopoulos, *Phys*. *Rev*. B **50**, 7488 (1994).

[12]   K. R. Allakhverdiev, T. G. Mammadov, R. A. Suleymanov, and N. Z. Gasanov, *J. Phys.: Condens. Matter* **5**, 1291 (2003).

[13]   K. R. Allakhverdiev, *Solid State Commun*. **111**, 253 (1999).

[14]   T. D. Ibragimov and I. I. Aslanov, *Solid State Commun*. **123**, 339 (2002).

[15]   Nevin Kalkan, M. P. Hanias, and A. N. Anagnostopoulos, *Mat. Res. Bull.* **27**, 1329 (1992).

[16]   G.D. Guseinov, E. Mooser, E.M. Kerimova, R.S. Gamidov, I. V. Alekseev, and M.Z. Ismailov, *Phys. Stat. Sol.* **34**, 33 (1969).

[17]   M. Ya. Bakirov, N.M. Zeinalov, S.G. Abdullayeva, V.A. Gajiyev, and E.M. Gojayev, *Solid State Commun.* **44**, 205-207 (1982).

[18]   A. Aydinli, N. M. Gasanly, I. Yilmaz, and A. Serpenguzel, *Semicond. Sci. Technol.* **14**, 599 (1999).

[19]   G. A. Gamal , *Semicond. Sci. Technol.* **13**, 185-189 (1998).

[20]   A. F. Qasrawi and N. M. Gasanly, *Phys. Stat. Sol.* **199**, 277-283 (2003).

[21]   V. M. Skorikov, V. I. Chmyrev, V. V. Zuev, and E. V. Larina, *Inorg. Mater.* **38**, 751 (2002).

[22]   Y. Kamitani and S. Maeta, *Jpn. J. Appl. Phys.* **39**, 115 (2000).

[23]   E. Borchi, M. Bruzzi, S. Pirollo, and S. Sciortino, *J. Phys. D: Appl. Phys.* **3**, L93 (1998).

[24]   R. Chen and Y. Kirsh, *Analysis of Thermally Stimulated Processes,* Pergamon Press, Oxford, (1981).

[25]   R. Bube, *Photoelectronic Properties of Semiconductors*, Cambridge University Press, Cambridge, (1992).

[26]   J.T. Randall and M.H.F. Wilkins, *Proc. Roy. Soc.* (London) **A 184**, 366, 390 (1945).

[27]   R.R. Haering and E.N. Adams, *Phys. Rev.* **117**, 451 (1960).

[28]   K.H. Nicholas and J. Woods, *Brit. J. Appl. Phys.* **15**, 783 (1964).

[29]   G.A. Dussel and R.H. Bube, *Phys. Rev.* **155**, 764 (1967).

[30]   S. Ozdemir, R. A. Suleymanov, E. Civan, and T. Firat, *Solid State Commun.* **98**, 385 (1996).

[31]   N. S. Yuksek, N. M. Gasanly, H. Ozkan, and O. Karci, *Acta Phys. Polonica* A **106**, 95 (2004).

[32]   N. A. P. Mogaddam, N. S. Yuksek, N. M. Gasanly, and H. Ozkan, *J. All. Comp.* **417**, 23 (2006).

[33]   C.Kittel, *Introduction to Solid State Physics,* Wiley, New York, (1971).

[34]   W. L. Bragg, *Proceedings of the Royal Society of London Series* A **17,** Part I, 43 (1913).

[35]   J. I. Pankove, *Optical Processes in Semiconductors*, Prentice Hall, New Jersey (1971).

[36]   T. S. Moss, G. J. Burrell, and B. Ellis, *Semiconductor Opto-Electronics*, John Wiley & Sons, New York (1973).

[37]   S. H. Wemple and M. DiDomenico, *Phys. Rev. Lett.* **23**, 1156 (1969).

[38]   K. Tanaka, *Thin Solid Films* **66**, 271 (1980).

[39]   S. W. S. McKeever, *Thermoluminescence of solids*, Cambridge Uni. Press, Cambridge (1985).

[40]   B. G. Markey, *Deep Level Characterization of Seeded Physical Vapor Transport Zinc Selenide* (PhD Thesis, Oklahoma, 1993).

[41]   N. S. Yuksek, N. M. Gasanly, and H. Ozkan, *Semicond. Sci. Technol.* **18**, 834 (2003).

[42]   T. A. T. Cowell and J. Woods, *Brit. J. Appl. Phys.* **18**, 1047 (1967).

[43]   C. Manfredotti, R. Murri, A. Quirini, and L. Vasanelli, *Phys. Stat. Sol.* (a) **38**, 685 (1976).

[44]   A. Serpi, *J. Phys. D: Appl. Phys.* **9**, 1881 (1976).

[45]   N. S. Yuksek, N. M. Gasanly, H. Ozkan, Progress in Condensed Matter Physics *"Thermally Stimulated Current Observation of Trapping Centers in Layered Thallium Dichalcogenide Semiconductors"*, Nova Science Publishers, Inc. (2004).

[46]   S. H. Wemple and M. DiDomenico, *Phys. Rev.* B **3**, 1338 (1971).

[47]   A. F. Qasrawi and N. M. Gasanly, *Phys. Stat. Sol.* (a) **202**, 2501 (2005).

[48]   J. A. Kalomiros, N. Kalkan, M. Hanias, A. N. Anagnostopoulos, and K. Kambas, *Solid State Commun.* **96**, 601 (1995).

[49] M. M. El-Nahass, M. M. Salam, S. A. Rahman, and E. M. Ibrahim, *Solid State Sci.* **8**, 488 (2006).

[50] Y. Shim, W. Okada, K. Wakita, and N. Mamedov, *J. Appl. Phys.* **102**, 083537 (2007).

[51] S. Ozdemir, N. M. Gasanly, and M. Bucurgat, *Phys. Stat. Sol.* (a) **196**, 422 (2003).

[52] A. Bosacchi, B. Bosacchi, S. Franchia, and L. Hernandez, *Solid State Commun.* **13**, 1805 (1973).

[53] A. Anedda, M. B. Casu, A. Serpi, I. I. Burlakov, I. M. Tiginyanu, and V. V. Ursaki, *J. Phys. Chem. Sol.* **58**, 325 (1997).

[54] P. C. Ricci, A. Anedda, R. Corpino, I. M. Tiginyanu, and V. V. Ursaki, *J. Phys. Chem. Sol.* **64**, 1941 (2003).

[55] T. Pisarkiewicz, *Opto-Electron. Rev.* **12**, 33 (2004).

[56] A.F. Qasrawi and N.M. Gasanly, *Cryst.Res.Technol.* **39**, 439 (2004).